Catalysis Science & Technology

Accepted Manuscript

This article can be cited before page numbers have been issued, to do this please use: J. S. Arora, K. B. Ansari, J. W. Chew, P. J. Dauenhauer and S. H. H. Mushrif, *Catal. Sci. Technol.*, 2019, DOI: 10.1039/C9CY00005D.

ROYAL SOCIETY OF CHEMISTRY

rsc.li/catalysis

View Article Online
DOI: 10.1039/C9CY00005D

Unravelling the Catalytic Influence of Naturally Occurring Salts on Biomass Pyrolysis Chemistry Using Glucose as a Model Compound: A Combined Experimental and DFT Study

Jyotsna S. Arora[†], *Khursheed B. Ansari*[†1], *Jia Wei Chew*[†], *Paul J. Dauenhauer*[‡], *Samir H. Mushrif*[§*]

[†]School of Chemical and Biomedical Engineering, Nanyang Technological University, 62 Nanyang Drive, Singapore 637459, Singapore

[‡]Department of Chemical Engineering and Materials Science, University of Minnesota, 421 Washington Ave. SE, Minneapolis, Minnesota 55455, United States

[§]Department of Chemical and Materials Engineering, University of Alberta, 9211-116 St NW, Edmonton, Alberta T6G1H9, Canada.

[*]Corresponding author, email: mushrif@ualberta.ca

Phone: 780-492-4872

Fax: 780-492-2881

[1] Current Affiliation: Department of Chemical Engineering, Aligarh Muslim University, AMU Campus, Aligarh 201002 Uttar Pradesh, India

View Article Online
DOI: 10.1039/C9CY00005D

Abstract

Fast pyrolysis is an efficient thermochemical decomposition process to produce bio-oil and renewable chemicals from lignocellulosic biomass. It has been suggested that alkali- and alkaline-earth metal (AAEM) ions in biomass alter the yield and composition of bio-oil, but little is known about the intrinsic chemistry of metal-catalyzed biomass pyrolysis. In this study, we combined thin-film pyrolysis experiments and density functional theory (DFT) calculations to obtain insights into AAEM-catalyzed glucose decomposition reactions, especially forming major bio-oil components and char. Experiments reveal the difference in the yield and composition of bio-oil of metal-free and AAEM complexed glucose. Metal-free glucose produced 2,3-dihydro-3,5-dihydroxy-6-methyl-4H-Pyran-4-one (DHMDHP) as the predominant compound in bio-oil, while 1,6-anhydroglucofuranose (AGF) maximized in Na(I)/glucose, levoglucosan (LGA) in K(I)/glucose, levoglucosenone (LGO) in Ca(II)/glucose and furfural in Mg(II)/glucose. To evaluate the stereoelectronic basis of metal ions in altering pyrolysis reaction kinetics, the reaction mechanisms of AGF, LGA, 5-hydroxymethylfurfural (5-HMF), furfural, 1,5-anhydro-4-deoxy-D-glycerohex-1-en-3-ulose (ADGH), LGO, and char formation were investigated using DFT calculations. DFT results showed that the presence of Ca(II) and Mg(II) ions catalyzed furfural and LGO formation, while alkali ions decatalyzed the formation of on these products. Conversely, Na(I) and K(I) ions catalyzed the concerted dehydrative ring closure of glucofuranose during AGF formation. For ADGH, AAEMs showed anti-catalytic effect. We also described a novel route for char formation via coupling between 1,2-anhydroglucopyranose and a carbonyl compound. The presence of alkali ions catalyzed char formation. Thus, the atomistic insights obtained from DFT calculations assist in understanding the observed change in experimental yields of individual bio-oil compounds governing its composition.

View Article Online
DOI: 10.1039/C9CY00005D

1. Introduction

Vast amounts of lignocellulosic biomass produced in nature can be potentially converted into renewable fuels without affecting the nutritional requirements of the world.[1] Utilization of the second generation lignocellulosic biomass can help in replacing fossil fuels, which, in turn, can reduce the emission of carbon dioxide and other greenhouse gases. Fast pyrolysis is a sustainable technology for generating renewable fuels/blends from biomass, compared to biochemical (i.e., fermentation) and gasification processes.[2, 3] In fast pyrolysis, biomass decomposes at high temperature (400-600 ^{o}C) in the absence of oxygen and generates bio-oil, along with non-condensable gases and char. Thermal deconstruction of polymeric biomass comprises of multiple reactions i.e., depolymerization, dehydration, ring fragmentation, and repolymerization, which generate a number of bio-oil components and solid char.[4, 5] The storage, handling, and direct utilization of bio-oil is hindered by its high oxygen and water content and therefore bio-oil requires further processing through deoxygenation/hydrodeoxygenation in the presence of a heterogeneous catalyst before it can be used as a fuel.[6]

Obtaining insights into the intrinsic reaction chemistry of biomass pyrolysis is crucial for developing the technology, because the yield and composition of bio-oil are governed by the reactions that take place in the condensed-phase. However, reaction chemistry, kinetics and transport effects are inter-related[7], which makes it difficult to study the intrinsic reactions of biomass pyrolysis under the given operating conditions. To deconvolute the effect of transport on pyrolysis reactions, advanced experimental methods like the thin-film technique have been developed.[7, 8] In thin-film experiments, biomass decomposition occurs in an isothermal, reaction-controlled regime, and insights into the fundamental chemistry of pyrolysis can be obtained by minimizing the secondary decomposition reactions.[8]

1.1 Understanding biomass pyrolysis chemistry: State of the art experiments

The underlying chemistry of biomass pyrolysis has been investigated for decades. The knowledge of pyrolysis reactions started with the global pathway of biomass/cellulose decomposition into gas, tar, and char, which was further improved as direct and indirect lumped pathways/mechanisms, and finally a component specific reaction mechanism was proposed. However, the prediction capability of these models remains limited considering the conventional trial and error approach taken in these studies. Further, the conventional pyrolysis system with allied analytical instruments has limitations in capturing the pyrolysis chemistry and kinetics due to the multiphase decomposition process with convoluted, fast chemistry and transport effects. However, recently advanced pyrolysis reactor systems such as CDS Pyroprobe,[9] micropyrolyzer,[7, 10, 11] wire-mesh reactor,[12] and Pulsed-Heated Analysis of Solid Reactions (PHASR)[13, 14] enhance the heating rate of thin-film biomass samples (heating rate ~ 200 – 12,000 ^{o}C.s^{-1}) compared to the conventional method (TGA, heating rate ~ 3 – 4 ^{o}C.s^{-1}).[15] The kinetics of cellulose conversion, measured using the PHASR reactor, deconvoluted the complex chemistry of cellulose decomposition and showed that intra-chain scission of cellulose, resulting in the formation of low-

molecular-weight volatiles, was favored above 467 °C, termed as the reactive melting point (T_{RM}), while below T_{RM}, chain-end mechanisms exhibited primary cellulose initiation reactions.[16] The effect of chain end type, i.e., presence of a reducing end vs. levoglucosan-end (LG-end) in the oligosaccharide, on the product distribution was investigated by Leng et al.[17] Their results suggested that the presence of a reducing-end in the sugar molecule favored ring opening reactions generating higher yield of furans, while the LG-end promoted dehydration reactions generating pyrans and secondary reaction products.[17] We recently discussed the decomposition chemistry of glucose under isothermal conditions at different operating temperatures (300-500 °C) and proposed a detailed reaction network map of glucose breakdown based on the change in the product yields with increasing temperature.[2]

Although, there are multiple experimental studies on cellulose decomposition, the experimental results can only provide macroscopic information about the decomposition process and insights into the formation of short-lived intermediates; reaction mechanisms are limited. Attempts to understand the reaction chemistry involved the use of isotopic labelling studies[18, 19] as well as *first principles* calculations[20-22]. Molecular modelling is an effective tool to understand the reaction mechanisms and kinetics.[3] Selected examples from the literature are as follows: Seshadri and Westmoreland investigated the pyrolysis of β-D-glucose and suggested concerted reaction pathways for several elementary reaction steps including dehydration, retro-aldol condensation and keto-enol tautomerization[23]. Hu et al. performed Density Functional theory (DFT) calculations to evaluate the lowest-energy pathways for the formation of 1,6-anhydroglucofuranose (AGF), 1,4,3,6-dianhydroglucopyranose (DAGP) and 1,5-anhydro-4-deoxy-D-glycerohex-1-en-3-ulose (ADGH).[20] Mayes et al. combined quantum mechanical calculations with experiments to evaluate the pathways for 5-hydroxymethylfurfural (5-HMF) formation and unimolecular 1,2-dehydration reactions of anomers α- and β-D-glucopyranose.[24] In summary, molecular simulations can provide a comprehensive understanding of the elementary steps that take place in the complex reaction network of cellulose pyrolysis.

1.2 Influence of inorganic metal salts on biomass pyrolysis

Except for few studies,[25-29] a majority of the experiments and multiscale theoretical calculations have been performed for individual biomass components with emphasis on glucose/cellulose decomposition [7, 8, 30, 31] because cellulose is the most abundant component of plant biomass comprising of an ordered polymeric structure of β-D-glucose units. However, biomass contains about 0.5–5 wt% alkali- and alkaline-earth metal (AAEM) salts.[26, 27] These metal salts are predominantly concentrated in the cells and partitioned into almost all subcellular compartments of leaves and roots of plant biomass. The presence of these inherent metal salts alter the yield and composition of bio-oil and char.[26, 27] Thermogravimetric analysis (TGA) and differential thermal analysis (DTA) of AAEM salts impregnated cellulose pyrolysis showed that the presence of alkali salts did not promote weight loss of the impregnated samples, which, in turn, was related to the dehydration and carbonization reactions during cellulose pyrolysis.[28] On the other hand, maximum yields of water from Mg(II) and Ca(II)-impregnated cellulose were obtained at lower

View Article Online
DOI: 10.1039/C9CY00005D

temperatures i.e., 200 ºC for Mg(II), while 250 ºC for Ca(II)-chloride compared to 350 ºC for untreated cellulose.[28] The effect of Na(I), K(I), Ca(II) and Mg(II) salts on primary pyrolysis product distribution of cellulose showed that chloride salts of Na(I) and K(I) result in a product distribution similar to that of untreated cellulose, while Mg(II) and Ca(II) chloride salts showed enhanced formation of furans and levoglucosenone (LGO).[27] Zhu et al. evaluated the overall yield and composition of volatile organic vapours and char by comparing the results of Ca(II) and Mg(II) loaded cellulose powder (diffusion-limited) and thin-film (isothermal reaction-controlled regime) pyrolysis experiments. Their results suggested that Ca(II) ions favored primary catalytic reactions of cellulose to char, while Mg(II) ions affected secondary char formation.[26] However, the reaction mechanisms and pathways proposed were based on the final product distribution.[26] Moreover, due to extremely fast timescales, the presence of multiple competing reactions and difficulty in measuring pyrolysis kinetics experimentally, insights into the intermediates and kinetics of reaction mechanisms in the presence of AAEMs cannot be obtained based on the final product distribution. Therefore, computational studies play a key role in understanding the reaction chemistry and also for developing the reaction map of metal-assisted biomass pyrolysis, which will be beneficial to comprehend the catalytic (or anti-catalytic) effect of metal salts on primary/secondary reactions of pyrolysis.

DFT calculations combined with experiments to study glucose decomposition in the presence and absence of Na(I) salt suggested that the presence of Na(I) ion stabilized the charged atoms of the transition state, which, lowered the activation barriers for levoglucosan (LGA) and a few dehydration reactions of glucose/ its intermediates. However, this study also hypothesized that other indigenous metal ions i.e., K(I), Ca(II) and Mg(II) have an effect similar to that of Na(I) ion on the reaction kinetics and product distribution.[25] Recently, we used DFT simulations to investigate the effect of Na(I), K(I), Ca(II) and Mg(II) ions on the glycosidic bond cleavage via six different mechanisms, categorized as direct glycosidic bond breaking pathways and two-step pathways to produce (precursors to) LGA and furans as products. The results highlighted that all four metal ions have different effects on the activation barriers of glycosidic bond breaking reactions.[32]

Although metal-assisted biomass pyrolysis has been studied in the past, few questions remain unanswered:

1. Do metal cations catalyze primary or secondary reactions of biomass decomposition?
2. Do all AAEMs exhibit similar (catalytic or anti-catalytic) effect on biomass pyrolysis chemistry?

To answer these questions, it is imperative to perform a comprehensive analysis of the chemistry for the formation of all major bio-oil components and char in the presence of all four AAEM ions.

Therefore, the present study is an attempt to bridge the aforementioned knowledge gaps and obtain molecular level information of the effect of AAEM cations on pyrolysis reactions and associated kinetics. In this work, we present an integrated experimental and theoretical approach to investigate AAEM catalyzed pyrolysis chemistry. Thin-film experiments of glucose pyrolysis are performed to

investigate the influence of alkali (Na(I) and K(I)) and alkaline-earth (Ca(II) and Mg(II)) metal ions (primarily found in biomass) on the yield and composition of bio-oil and char. β-D-glucose is used as model biomass compound, because glucose is the monomer of cellulose and also one of the intermediates formed during cellulose pyrolysis. Next, atomistic insights into the reaction chemistry of AAEM-catalyzed glucose decomposition generating major bio-oil components and char are obtained using DFT calculations.

The methodology for thin-film sample preparation and details of pyrolysis experiments are presented in Section 2. Section 3 describes the methods used for molecular simulations to investigate metal ion catalyzed-glucose decomposition reactions forming bio-oil components and char. In Section 4.1, the product yields of bio-oil and char obtained from glucose thin-film pyrolysis experiments in the presence and absence of AAEM salts at 200 ºC are discussed. In the latter part of section 4.1, we briefly discuss the integrated approach taken in the current study i.e., we correlate the experimentally observed yield of individual bio-oil components and char with DFT-calculated activation barriers along the reaction pathways. In section 4.2, we describe the binding sites of AAEM ions with glucose to obtain the most stable configurations of metal-glucose complexes. The reaction map of glucose decomposition is discussed in section 4.3, and section 4.4 gives the results and discussion of the DFT calculations for the formation of bio-oil components, namely, 1,6-anhydroglucofuranose (AGF), 1,5-anhydro-4-deoxy-D-glycerohex-1-en-3-ulose (ADGH), levoglucosan (LGA) and levoglucosenone (LGO); 5-hydroxymethylfurfural (5-HMF), furfural and char. Finally, we summarize the findings of this work in section 5.

2. Materials and Methods

2.1. Materials used and Sample Preparation

Glucose (Lot No: G8270) and metal salts i.e., sodium chloride (Lot No: 746398), potassium chloride (Lot No: 746436), magnesium chloride (Lot No: M2670) and calcium chloride (Lot No: 746495) were purchased from Sigma Aldrich, Singapore. Initially, glucose thin-films were prepared by dissolving 1.0% (weight basis) of glucose in deionized (DI) water. Then, 25 μL of 1.0 wt % clear glucose solution was transferred into a cylindrical pyrolysis crucible; 4 mm × 8 mm (diameter × height) in size. The water was then removed *via* room temperature evacuation, leaving behind a micrometer-sized film of glucose on the inner wall of the crucible.[2, 7, 11]

To study the effect of AAEMs, glucose was mixed with metal salts individually i.e., NaCl, KCl, $MgCl_2$ and $CaCl_2$. The required amount of NaCl, KCl, $MgCl_2$ and $CaCl_2$ (0.35 mmol metal salt/g of glucose)[27] was measured and then was added to 1.0 g of glucose; followed by deionized water addition which yielded a ~1.0 wt% clear solution of glucose homogeneously mixed with metal salts. A similar procedure of water evaporation, as mentioned above, was followed which generated a micrometer-sized film of glucose/metal salts. The thickness of the films was measured using a digital microscope (Leica DVM6) and are shown in Fig. 1[**A**] and 1[**B**]. The image analysis showed that glucose films in the

View Article Online
DOI: 10.1039/C9CY00005D

presence and absence of AAEMs were 10–12 μm thick, which exist inside the reaction-controlled regime of experimental pyrolysis.[11] The method of glucose thin-film preparation and its thickness measurement are also reported elsewhere.[2]

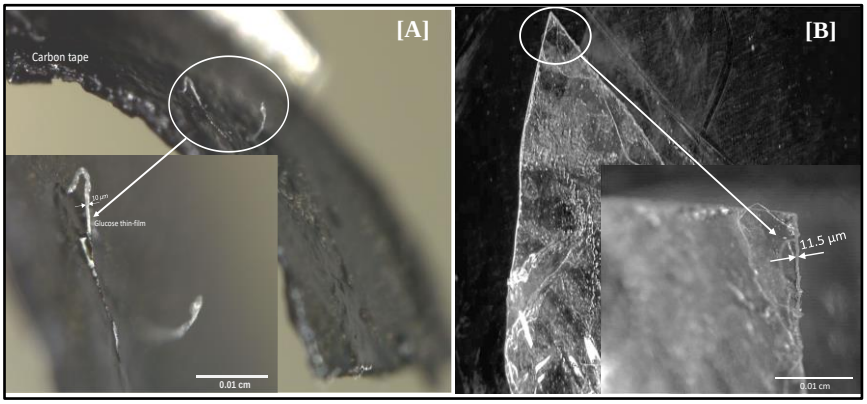

Figure 1: Thin-film images acquired from Leica DVM6 digital microscope [**A**] Glucose thin-film without metal [**B**] Glucose thin-film with 0.35 mmol magnesium chloride/g of glucose

2.2. Pyrolysis Experiments

Thin films of metal-free glucose and homogeneously mixed glucose with AAEMs (NaCl, KCl, $MgCl_2$ and $CaCl_2$) were pyrolyzed using a micropyrolyzer (PY-3030S single shot pyrolyzer, Frontier Laboratories Ltd., Japan) at 200 ºC. The operating temperature for pyrolysis experiments was selected as 200 ºC as the melting point of glucose is 146-150 ºC, therefore at 200 ºC, only primary reactions of glucose decomposition in the presence and absence of the metal ion will be predominant. This in-turn generated few (~ 9–11) volatile compounds along with char, thus minimizing secondary reactions of the intermediates and/or primary products, which assisted in evaluating the direct influence of metal ion(s) on pyrolysis reactions. Moreover, the temperature of glucose thin-film samples were raised by ~1,000,000 °C/min, in the micropyrolyzer, which is three-to-five orders of magnitude faster than traditional heating rates in pyrolysis techniques.[2, 11, 33] This allowed glucose thin-film samples to decompose under an isothermal and reaction-controlled regime. Thus, the pyrolysis product distribution obtained is a representation of the intrinsic chemistry of glucose decomposition (free of transport-limitations).

Pyrolysis volatile products were immediately transferred (using a continuous flow of helium gas) to a gas chromatograph (Agilent, Model 7890B) coupled with a mass spectrometer (Model 5977B MSD) for identification and quantification. Post reaction, the solid residue of pyrolysis (char) was quantified *via* combustion by injecting the oxygen pulse into the micropyrolyzer.[2, 7, 11] The volatile products were identified using both mass spectrometry and by comparing retention times (RT) of these compounds to that of pure standards. The compounds, such as 1,4,3,6-dianhydroglucopyranose (DAGP); 1,6-anhydroglucofuranose (AGF); 1,5-anhydro-4-deoxy-D-glycerohex-1-en-3-ulose (ADGH); 2,3-dihydro-3,5-dihydroxy-6-methyl-4HPyran-4-one (DHMDHP); and 1,2-cyclopentanedione (CPD) were

View Article Online
DOI: 10.1039/C9CY00005D

quantified using previously reported method.[2] Pyrolysis experiments of glucose thin-films in the presence and absence of metal salts were conducted in triplicate and the average values (product yields, % C basis) are shown in the results and discussion section 4.1 with the experimental error. The standard deviation in individual product yield ranged between 1–2 %. The overall carbon balance for thin-film pyrolysis of glucose/metal salts, including volatile products and char, was 82-90%.

3. Computational Methodology

All-electron DFT calculations were performed using Gaussian *09* code.[34] The 6-311++G(2d,p) basis set with the hybrid M06-2X functional was used in the present study as it provided accurate estimates of energy barriers for carbohydrate chemistry.[20, 24, 25] No constraints were implemented on the atoms during geometry optimizations and transition state (TS) search. The Berny algorithm, as implemented in the Gaussian code, was used for the TS search. Geometry optimizations were followed by frequency calculations to differentiate between the saddle points and local minima on the potential energy surface i.e., the TSs and ground state structures, by the presence and absence of an imaginary frequency, respectively, which relates to the reaction coordinate. Next, intrinsic reaction coordinate (IRC) calculations were performed to verify that the molecular structure of the obtained TS linked with the anticipated reactant and product on the potential energy surface.

Glucose is chosen as the model compound in the present study as it is the monomer of cellulose and an important intermediate that is formed during cellulose pyrolysis.[35] The Polarizable Continuum Model (PCM) using the integral equation formalism variant (IEFPCM) was taken into account for all the geometry optimization and TS search calculations intended for emulating the condensed phase of cellulose pyrolysis. Ethanol was used as the implicit solvent in the continuum model. This is because the dielectric constant (ε) of EtOH (24.85) is comparable to that of glucose (21.0) at 200 °C.[36]

The electronic properties and the bonding character of AAEM ions with glucose/intermediates/the TS(s) were evaluated using the Natural Bond Orbital (NBO) analysis. For evaluating metal-glucopyranose and metal-intermediate complexation, the metal ion was complexed with various oxygen atoms in glucopyranose and the intermediate (formed in a multi-step reaction). Enthalpy of complexation ($\Delta H_{complxn}$) is calculated using eqn (1).

$$\Delta H_{complxn} = H_{complx} - (H_{glucopyran} + H_{metal-ion}) \quad (1)$$

The metal coordinated structure which results in the most favourable $\Delta H_{complxn}$ was taken as the ground state reactant/intermediate complex and was used for activation barrier calculations. Figure 2 shows the atom numbering in β-D-glucopyranose (**1**). The oxygen atom bonded to the carbon have that carbon's number. Similarly, the hydrogen attached to the oxygen has that oxygen's number, while the hydrogen atoms attached to carbon are numbered sequentially from H_7 to H_{13}, commencing from C_1. Throughout the discussion, the atoms will be referred to by this nomenclature. In addition to this, the

View Article Online
DOI: 10.1039/C9CY00005D

reactant, intermediate(s) and products from each reaction pathway are assigned a specific number (written in parenthesis), while each TS is given a label, e.g. AG-ts1, where the first two letters 'AG' indicate the chemical species i.e., anhydroglucofuranose, while 'ts1' indicates the transition state of step-number 1 in a multi-step reaction. This label is written on the reaction arrow of each reaction pathway. The enthalpic activation barriers, reported in kcal.mol^{-1}, were computed at 1.0 atm and 200 °C.

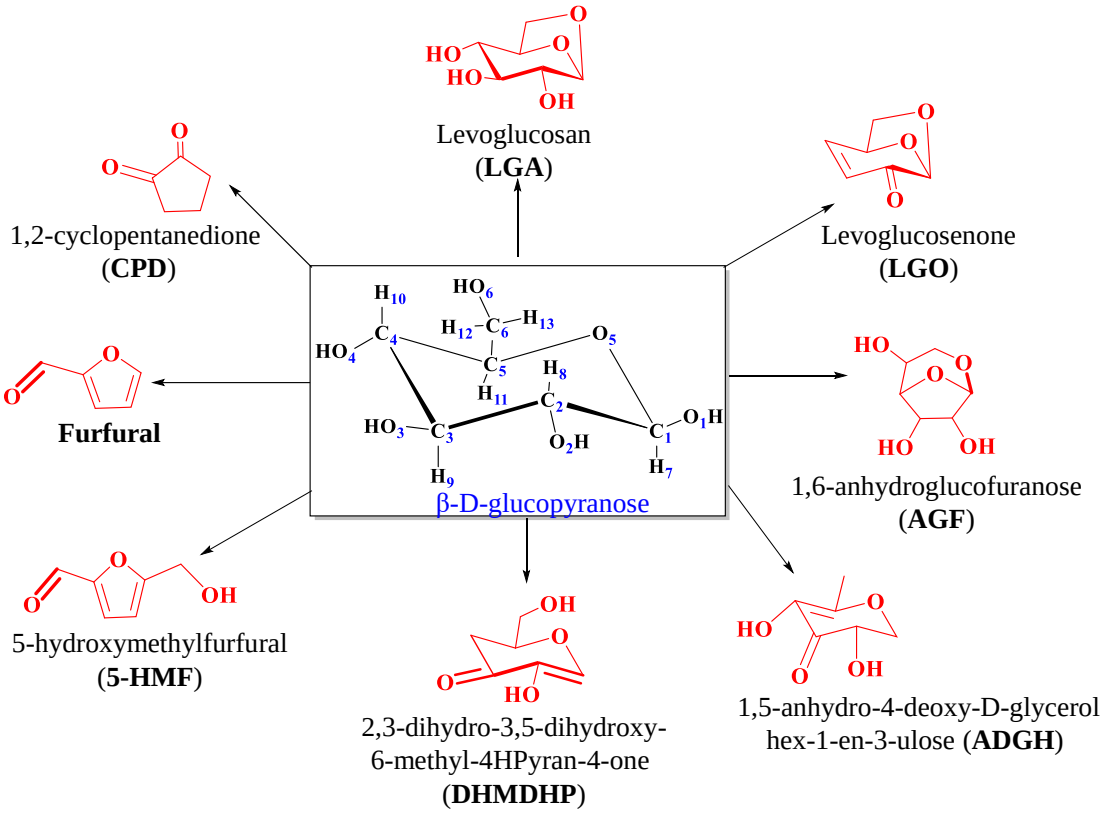

Figure 2: Major compounds (bio-oil components) obtained from the pyrolysis of β-D-glucopyranose in metal-free conditions. The atom numbering scheme in β-D-glucopyranose (**1**) is also shown.

4. Results and Discussion

4.1 Glucose thin-film pyrolysis with and without metal salts: Product distribution and bio-oil composition

Figure 3[**A**] shows bio-oil and char yields in the presence and absence of AAEM ions. Thin-film pyrolysis of glucose without metal salts at 200 ºC produced 20.93 ± 0.18 % of bio-oil and 61.71 ± 1.05 % char. Pyrolysis of Mg(II) and Ca(II) /glucose thin-film produced similar yields of bio-oil (~ 20.5 %) and char (~ 62.05 %), while Na(I)/glucose and K(I)/glucose thin-films decreased bio-oil yield by 2-6%, which, in turn, increased char yield by 9-10%.

The bio-oil so formed is comprised of anhydrosugars, namely levoglucosan (LGA) and 1,6-anhydroglucofuranose (AGF); pyrans: 1,5-anhydro-4-deoxy-D-glycerohex-1-en-3-ulose (ADGH) and

2,3-dihydro-3,5-dihydroxy-6-methyl-4HPyran-4-one (DHMDHP); furans i.e., furfural, 5-hydroxymethylfurfural (5-HMF), furan and 5-methylfurfural, as well as light oxygenates like 1,2-cyclopentanedione (CPD). In the absence of the metal ions, the highest yields from glucose pyrolysis were of DHMDHP (~ 8 %), followed by LGA (~ 7%), furfural (~ 2.6 %) and then ADGH and AGF (~ 1.2 %). 5-HMF, furan, 5-methylfurfural and CPD were obtained in lower yields (< 1 %) and remained as minor products. Figure 3[**B**] shows major products of glucose thin-film pyrolysis in the presence and absence of AAEMs at 200 ^{o}C. Table S1 of the supporting information lists the complete product distribution of glucose pyrolysis.

In the bio-oil obtained from Mg(II)/glucose thin-film pyrolysis, anhydrosugars comprised of levoglucosenone (LGO) and 1,4,3,6-dianhydroglucopyranose (DAGP) were additional products along with LGA and AGF. Presence of Mg(II) does not exhibit a significant change in AGF yield, while LGA yield increased by 2 %, as compared to metal-free glucose. Furans such as furfural also increased by 4.5 % for Mg(II)/glucose thin-film, while DHMDHP and ADGH decreased by 7 % and 1 %, respectively, compared to the yields of these components obtained from pure glucose. Among minor products for Mg(II)/glucose, furan and 5-methylfurfural increased, while 5-HMF and CPD decreased. Further, the comparison of bio-oil components from Ca(II)/glucose with metal-free glucose pyrolysis showed that the yields of AGF in the presence of Ca(II) increased by 2.8 %, while LGA decreased by 1.2%. Similar to Mg(II)/glucose thin-film pyrolysis, LGO (~ 3.8 %) and DAGP (~ 0.5 %) were obtained as additional anhydrosugar compounds in the bio-oil of Ca(II)/glucose. Furfural in the bio-oil also increased by 2.8 % for Ca(II)/glucose, while no significant change in 5-HMF yield was observed for Ca(II)/glucose when compared to product distribution from pure glucose pyrolysis. Pyrans viz. DHMDHP and ADGH decreased by 6.7 % and ~ 1 %, respectively, in Ca(II)/glucose.

In the bio-oil from Na(I)/glucose and K(I)/glucose pyrolysis, anhydrosugars included LGA and AGF only; no LGO and DAGP were observed. This trend is similar to that shown by metal-free glucose. Further, LGA yield decreased by 2 % and 1.2 %, respectively, in the presence of Na(I) and K(I) ions. The yield of AGF was the highest (~ 3.8 %) in the presence of Na(I) ions, while AGF yield slightly decreased to ~ 3.4 % in the presence of K(I) ions. Furfural increased marginally (~ 0.5 and 1.5 % for Na(I) and K(I) ions, respectively), while HMF and 5-methylfurfural, remained unchanged for Na(I) and K(I)/glucose pyrolysis compared to that of metal-free glucose. The yield of pyrans, viz., DHMDHP and ADGH from Na(I) and K(I) assisted glucose pyrolysis also decreased by 5-6 % and 0.6 %, respectively, compared to their yields in the absence of metal ion.

Similar to Na(I)/glucose pyrolysis, anhydrosugars generated from K(I)/glucose pyrolysis comprised of LGA and AGF only. Further, LGA yield decreased by about 1.2 %, while furfural yield increased by 1.5 % compared to that of metal-free glucose. The yield of ADGH and DHMDHP also decreased by about 0.6 % and 5.5 %, respectively, during K(I)/glucose pyrolysis.

View Article Online
DOI: 10.1039/C9CY00005D

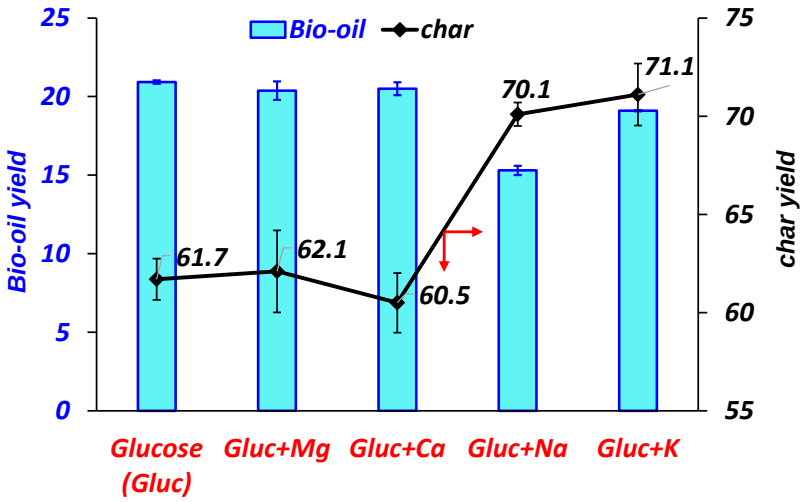

[**A**]

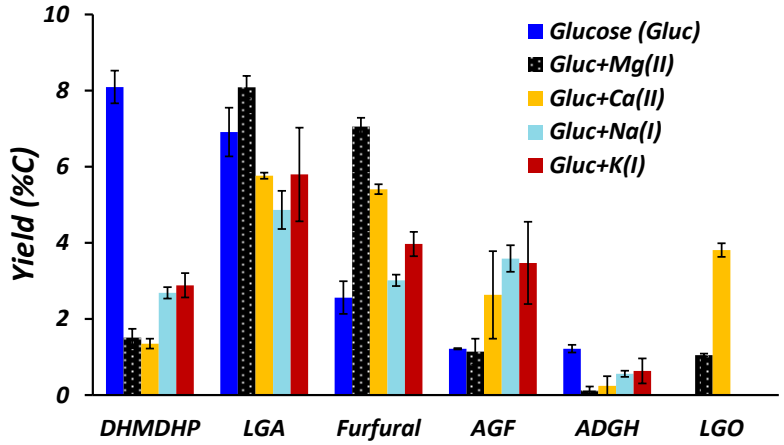

[**B**]

Figure 3: [**A**] shows bio-oil and char yields and [**B**] shows major bio-oil components from glucose thin-film pyrolysis, in the presence and absence of alkali and alkaline-earth metal salts at 200 °C. The metal salt loading is 0.35 mmole /g of glucose at 200 °C. [Nomenclature for pyrolysis products: **DHMDHP**: 2,3-dihydro-3,5-dihydroxy-6-methyl-4H-Pyran-4-one; **LGA**: levoglucosan; **AGF**: Anhydroglucofuranose; **ADGH**: 1,5-anhydro-4-deoxy-D-glycerohex-1-en-3-ulose and **LGO**: Levoglucosenone]

In summary, our experimental results show that Mg(II)/glucose pyrolysis resulted in the highest yield of furfural, while, Ca(II)/glucose produced more LGO than metal-free glucose. Further, Na(I)/ glucose resulted in a higher yield of AGF, while K(I)/glucose thin-film resulted in the highest yield of LGA. Interestingly, DHMDHP, the major product from metal-free glucose decomposition, decreased significantly in the presence of AAEM ions. Thus, it is evident from experiments that the presence of metal ions influences glucose pyrolysis product distribution differently, especially the yield and composition of bio-oil. Therefore, to evaluate the change in the reaction chemistry and kinetics brought

View Article Online
DOI: 10.1039/C9CY00005D

about by the complexation of metal ions with the reactant/intermediates/the TS, DFT calculations were performed.

Thermal decomposition reactions of metal/glucose complexes were computed using DFT to understand the stereoelectronic basis of the AAEM ions on the intrinsic chemistry of glucose pyrolysis. Numerous elementary reaction mechanisms have been proposed in the literature for the formation of 5-HMF, LGA and AGF[20, 21, 23, 24]. To investigate the catalytic (or anti-catalytic) effect of metal ions on the reaction pathways of LGA, AGF, ADGH, furfural and 5-HMF formation, only those reaction pathway(s) that are kinetically favored over other reported mechanisms described in the literature were computed in the present study. The activation barriers from these calculations were then correlated with the experimental yields of bio-oil components and char so as to obtain atomistic insights into the reaction chemistry of AAEM-catalyzed glucose decomposition.

4.2 Coordination complexes of alkali- and alkaline-earth metal ions with β-D-glucopyranose

The positively charged AAEMs Na(I), K(I), Ca(II) and Mg(II) ions coordinate with the electron-rich hydroxyl and pyranose oxygen atoms of β-D-glucopyranose (**1**). The stability of the metal/sugar complex is governed by the coordination site of the sugar molecule with the metal ion.[37] Na(I) ion was chosen as the model ion to investigate the most suitable coordination site for the complexation of metal ions with glucose. The stable metal-glucose complexes will be used as a reference point or starting structures to evaluate the activation barriers of glucose decomposition reactions in the presence of AAEMs. NBO charge distribution of β-D-glucopyranose (**1**) shows that hydroxyl groups possess slightly higher electronic charge (i.e., -0.75-0.77 au) compared to the ether oxygen atom having atomic charge of -0.65 au. Hence, there are four possible sites for the Na(I) ion to coordinate with β-D-glucopyranose (**1**), which are O_1 , O_2 categorized as **site1**; O_3 , O_4: **site2**; O_4 , O_6: **site3** and O_5 , O_6: **site4**. Figure 4[**A**] shows the NBO charge distribution of (**1**). Table 1 lists the complexation enthalpies of Na(I) ion coordinated at all the four sites.

The **sites 2** and **4** result in similar activation enthalpies of -5.11 and -5.13 kcal.mol^{-1}, respectively, for Na(I) ion coordination with β-D-glucopyranose. On the other hand, Na(I)/glucose complexes at **sites 1** and **3** have complexation enthalpies of -4.55 and -3.26 kcal.mol^{-1}, respectively. This is because **site1** Na(I)/glucose complex exhibits lesser charge transfer between Na(I) ion and O_1 , O_2 donor atoms, while Na(I)/glucose **site3** complex is devoid of an intramolecular H-bond between H_6 and O_5 atoms compared to the coordination structures of Na(I)/glucose at **site2** and **site4**. Literature studies discussed that metal (aquo) chloride/hydroxide complexes preferred to complex with C_1 and C_2 oxygen atoms of glucose.[38] However, the reported complexation studies were evaluated in the aqueous phase/in the presence of a solvent as opposed to the condensed-phase environment observed during pyrolysis, which in turn, resulted in different binding sites of the metal ion with β-D-glucopyranose. Figures 4[**B**] to 4[**E**] show Na(I)/β-D-glucopyranose-coordination complexes at **sites 1** to **4**.

View Article Online
DOI: 10.1039/C9CY00005D

Table 1: Complexation enthalpies (ΔH_{complx}) of Na(I) ion with β-D-glucopyranose

Molecular structure of glucose-Na(I) complex*	Oxygen atoms	Site	ΔH_{complx}, kcal.mol^{-1}
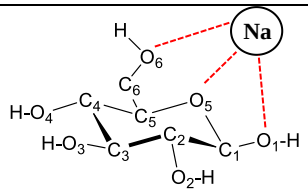	O_1, O_2	1	-4.55
	O_3, O_4	2	-5.11
	O_4, O_6	3	-3.26
	O_5, O_6	4	-5.13

*Representation of Na(I)-glucose coordination complex

Following the Na(I)/β-D-glucopyranose complexation studies, the coordination of K(I), Ca(II) and Mg(II) ions with β-D-glucopyranose at **sites 2** and **4** was evaluated. It was observed that the divalent Mg(II) and Ca(II) ions preferred to coordinate at **site4** (O_5, O_6) over **site2** (O_3, O_4), while Na(I) and K(I) ions exhibited similar complexation enthalpies at both **sites 2** and **4**. Mg(II) and Ca(II) ions coordinated at **site4**, had complexation enthalpies of -23.2 and -11.7 kcal.mol^{-1}, respectively; while Na(I) and K(I) ions showed complexation enthalpies of -5.13 and -5.88 kcal.mol^{-1}, respectively. Higher relative stability of divalent ions glucose complexes over alkali-ion complexes was because of divalent metal ions' higher charge density, which enabled stronger coordination of divalent metal ions with oxygen atoms. Table 2 summarizes the complexation enthalpies of metal ions with **sites 2** and **4** oxygen atoms and also lists the changes in geometrical parameters of β-D-glucopyranose on metal coordination and change in NBO charges of metal ion after complexation with glucose.

The C(1)-O(5) and C(5)-O(5) bonds elongate by 0.015–0.04 Å in Mg(II)/glucose-**site4** complex (**1**+**Mg(II)**) compared to the C-O bond lengths of β-D-glucopyranose. This implies the prospect of π-back donation from the metal ion to β-D-glucopyranose, thus stabilizing the Mg(II)/glucose-**site4** complex. In contrast, the remaining metal complexes showed that the C-O bond lengths get minimally altered (~0.02 Å) which indicated lower stability.

In summary, the stable metal/glucopyranose configurations serve as ground-state reactant complexes for evaluating the activation enthalpies of glucose decomposition. Further, insights into AAEM-glucopyranose coordination complexes suggest that binding of AAEMs with oxygen atoms of glucopyranose stabilize the metal/glucopyranose coordinate complexes, which in turn, can provide stability to the energy intensive transition states of the reaction. However, the binding site of AAEMs in the TSs may not be the same as its binding in the ground-state complexes. This is because the TS involves a change in the electronic/bonding properties of the atoms involved in the reaction, which, in turn, governs the binding of the metal ion in the TS. The details of metal binding in the TS and the intermediate species generated during the reaction pathway are discussed in section 4.4.

View Article Online
DOI: 10.1039/C9CY00005D

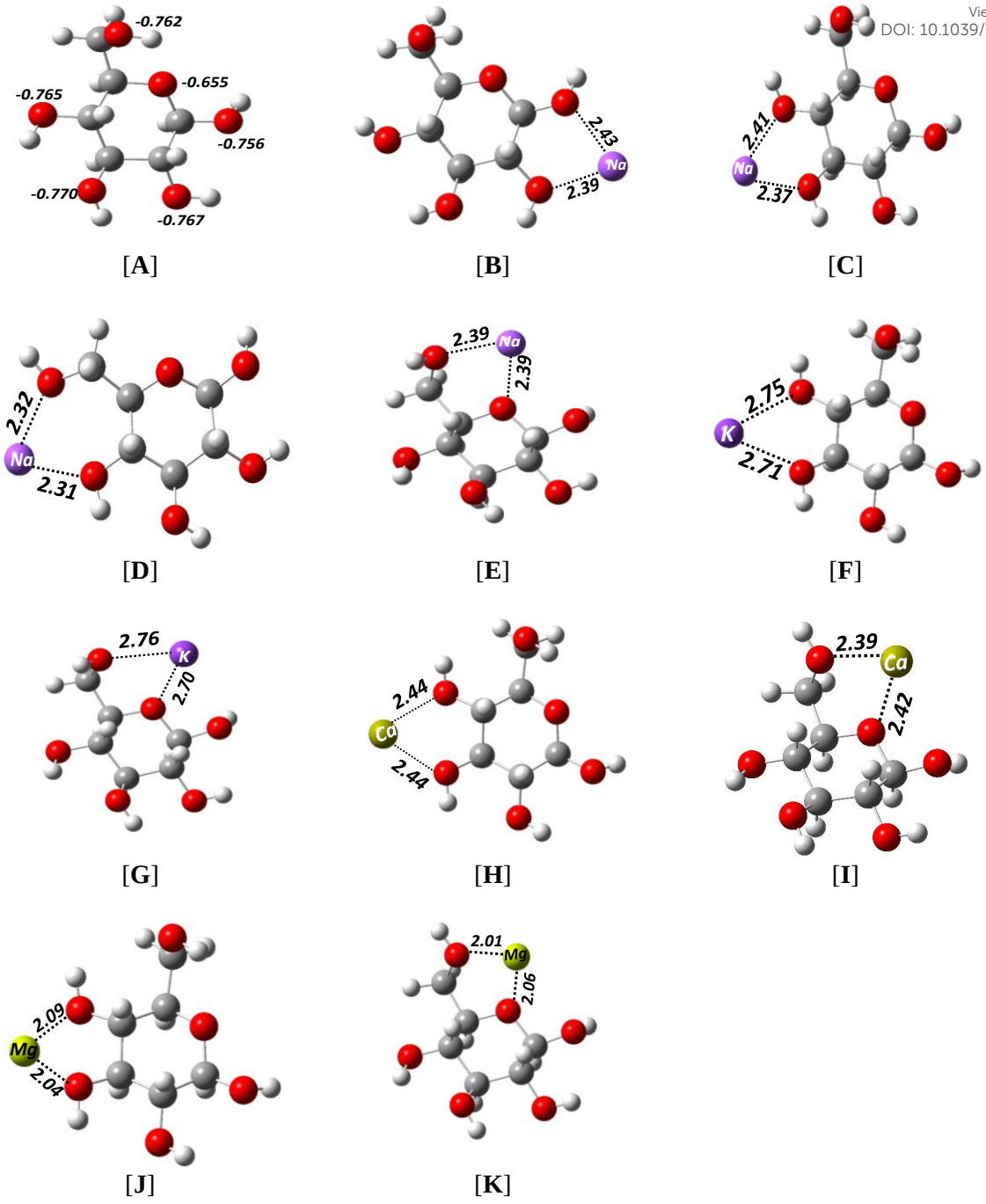

Figure 4: [**A**] Charge distribution in β-D-glucopyranose (au); [**B**] Na(I) ion coordination with O_1, O_2 atoms: **site1**; [**C**] Na(I) ion coordination with O_3, O_4 atoms: **site2**; [**D**] Na(I) ion coordination with O_4, O_6 atoms: **site3** [**E**] Na(I) ion coordination with O_5, O_6 atoms: **site4**; [**F**] K(I) ion coordination at **site2**; [**G**] K(I) ion coordination at **site4**; [**H**] Ca(II) ion coordination at **site2**; [**I**] Ca(II) ion coordination at **site4**; [**J**] Mg(II) ion coordination at **site2**; [**K**] Mg(II) ion coordination at **site4**. The units of the highlighted distances are Å. Grey, red and white balls indicate C, O, and H atoms, respectively.

View Article Online
DOI: 10.1039/C9CY00005D

Table 2: Enthalpies of complexation of alkali- and alkaline-earth metal ions with β-D-glucopyranose (**1**) at **sites 2** and **4**. Changes in the geometrical parameters, Natural Bond Order (NBO) charges of metal ion, and difference in the formal and NBO charge of the metal after complexation with β-D-glucopyranose at **site4** are listed.

	(1)	**(1)+Mg(II)**	**(1)+Ca(II)**	**(1)+Na(I)**	**(1)+K(I)**
Atoms of β-D-glucopyranose involved in metal ion coordination			Enthalpy of complexation (kcal.mol^{-1})		
Site2: O(3) & O(4)	--	-21.9	-11.1	-5.11	-5.31
Site4: O(5) & O(6)	--	-23.2	-11.7	-5.13	-5.88
[a] Geometrical parameters of **site4** complexes					
C(1)-O(1) [Å]	1.387	1.372	1.382	1.385	1.388
C(1)-O(5) [Å]	1.414	1.454	1.435	1.421	1.418
C(5)-O(5) [Å]	1.423	1.442	1.434	1.426	1.424
C(6)-O(6) [Å]	1.146	1.442	1.434	1.425	1.423
q_{metal} [au]		1.957	1.971	0.986	0.988
[b](M^{n+}) - (q_{metal})		0.043	0.029	0.014	0.012

[a] The units of geometrical parameters and NBO charge are written in square brackets; [b] formal charge on the metal ion before complexation with β-D-glucopyranose.

4.3: Reaction Map of Glucose Decomposition

Figure 5 shows the reaction network of glucose pyrolysis, resulting in the formation of experimentally observed products i.e., AGF, ADGH, LGA, LGO, 5-HMF, furfural, and char.

The formation of AGF from β-D-glucopyranose (**1**) involves cleavage of the 1,5-acetal bond to form acyclic D-glucose (**2**). 1,4-acetal bond formation in D-glucose (**2**) generates β-D-glucofuranose (**3**). The glucofuranose moiety (**3**) forms 1,6-acetal bond with loss of water in a concerted fashion resulting in AGF (**4**).[23, 39, 40]

ADGH formation from β-D-glucopyranose (**1**) takes place by the loss of a water molecule i.e., O_1H and H_2 atoms generating 1,2-anhydroglucopyranose (**5**). 1,2-anhydroglucopyranose (**5**) can further undergo dehydration i.e., loss of H_3 and O_4H generating intermediate (**6**), which subsequently undergoes tautomerization of enol group at C_3 forming ADGH (**7**). LGA (**8**) formation from β-D-glucopyranose (**1**) can follow two pathways. The first reaction pathway involves loss of water i.e., -O_1H and H from O_6 followed by ring closure of O_6 at C_1 in a concerted manner.[23] The second reaction pathway for LGA formation consists of isomerization of 1,2-anhydrolucopyranose (**5**). Under pyrolysis conditions, LGA is unstable and reactive.[41] LGO, a secondary reaction product of LGA decomposition[41], is formed by loss of water molecule i.e., H_2 and O_3H atoms from LGA (**8**) resulting in the formation of an enol intermediate (**9**), which generates a ketone intermediate (**10**) and finally another loss of water molecule H_8 and O_4H groups forming LGO (**11**).

The reaction pathway for 5-HMF formation from β-D-glucopyranose (**1**) involves a series of ring opening and dehydration reactions. Two routes for keto-intermediate (**15**) formation are possible[24].

Route one involves D-fructose (**12**) as an intermediate (path shown in black (**2**)-(**15**)), while route two involves cyclization D-glucose (**2**) with water loss (pathway shown in brown (**2**) to (**15**)). Furthermore, the ketone intermediate (**15**) also exhibits two competing routes for 5-HMF (**18**) formation i.e., loss of the first water molecule can occur from C_β of aldehydic group (path in green (**15**) to (**16**)) or from C_β of alcoholic group (path in black (**15**) to (**17**)). Further, the most favourable path for furfural (**19**) formation is by deformylation of 5-HMF.[25]

Char formation is a convoluted process and predominantly involves dehydration and bimolecular condensation reactions of C5 molecules and dehydrated volatile products/intermediates.[22] The primary OH group in 1,2-anhydroglucopyranose (**5**) can attack electron deficient C of C5 species (*e.g.* furfural or 5-HMF) by nucleophilic addition reaction to form an α,β-diol intermediate Ch-int1 (**20**). The Ch-int1 intermediate then undergoes dehydration, forming two enol intermediates, namely Ch-int2G (**21**) and Ch-int2F (**22**). The next step involves tautomerization of the enol generating ketone intermediates i.e., Ch-int3G (**23**) and Ch-int3F (**24**). The ketone intermediates are highly reactive due to the presence of α-H atoms and hence can further react with a carbonyl intermediate or can undergo nucleophilic addition reaction with the primary hydroxyl group of an intermediate/product. A series of reactions of ketone intermediates can take place in the pyrolysis condensed-phase thus contributing to char.

After mapping out the plausible route of glucose decomposition chemistry, molecular insights into the catalytic/ anti-catalytic effect of AAEM ions for the formation of AGF (**4**), ADGH (**7**), LGA (**8**) LGO **(11)**, 5-HMF (**18**), furfural (**19**) and **char** were investigated.

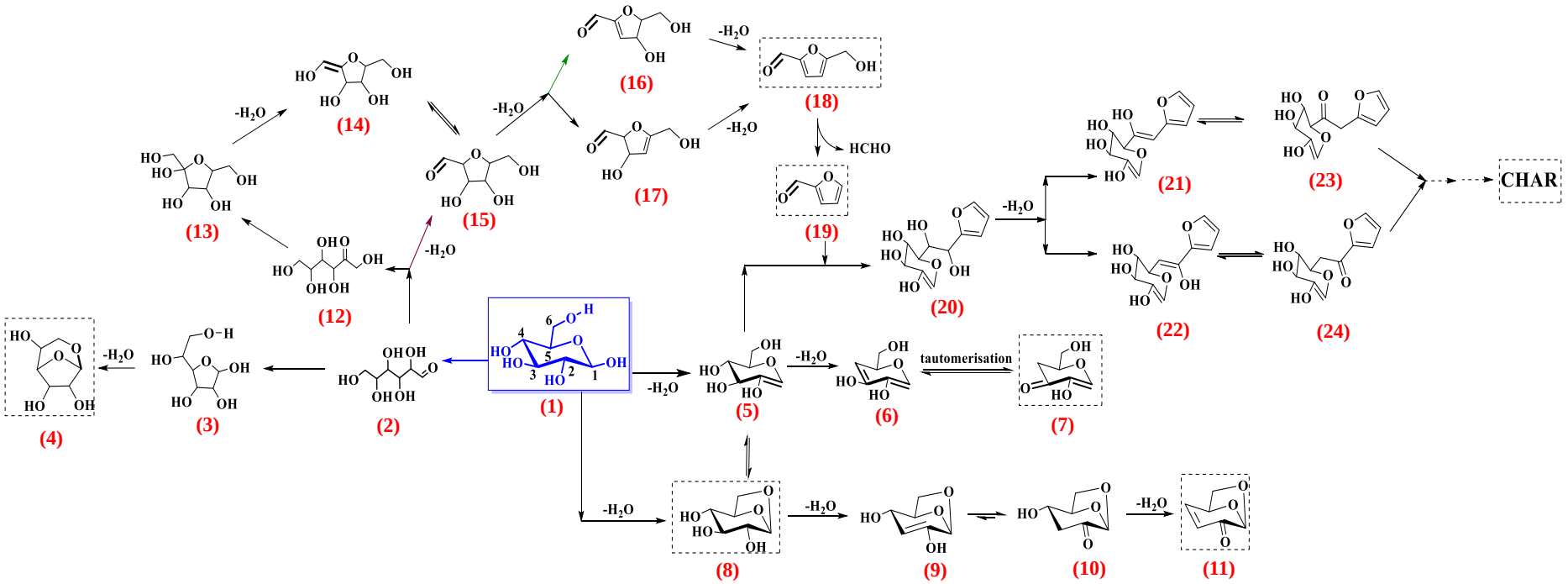

Figure 5: Reaction network of β-D-glucopyranose decomposition to form bio-oil components anhydroglucofuranose **(4)**, 1,5-anhydro-4-deoxy-D-glycerohex-1-en-3-ulose **(7)**, levoglucosan **(8)**, levoglucosenone **(11)**, 5-hydromethylfurfural **(18)**, furfural **(19)** and **char**. The numbers in parenthesis indicate the intermediate/product components formed during the course of the reaction. β-D-glucopyranose is shown in blue. The product components observed experimentally are shown inside the dashed box.

View Article Online
DOI: 10.1039/C9CY00005D

4.4: Mechanistic pathways of metal/glucose decomposition reaction chemistry

DFT calculations were performed to gain insights into the reaction kinetics and understand the stereoelectronic basis of the metal cation when coordinated to the energy-intensive transition state of the reaction pathway.

4.4.1: *Formation of Anhydroglucofuranose (AGF)*

The formation of AGF from β-D-glucopyranose (**1**) involves ring opening to form acyclic D-glucose (**2**), followed by 1,4-acetal bond formation in (**2**) generating β-D-glucofuranose (**3**), which, in turn, undergoes 1,6-acetal bond with loss of water in a concerted fashion, resulting in AGF (**4**).[23, 39, 40] Formation of β-D-glucofuranose (**3**) is the most crucial step responsible for AGF formation.[20] DFT computed activation enthalpies of the three steps involved in AGF formation i.e., AG-ts1, AG-ts2 and AG-ts3 are 45.4, 38.3 and 54.7 kcal.mol^{-1}, respectively, in the absence of metal ions. The activation enthalpy values indicate that 1,6-acetal bond formation accompanied by the loss of a water molecule, i.e., AG-ts3, is the rate-determining-step during AGF formation from glucopyranose. Therefore, the relative change in activation enthalpies of the rate-limiting step in the presence and absence of AAEMs is compared with the relative change in AGF experimental yields. Figure 6 shows the reaction scheme for the conversion of β-D-glucopyranose to AGF and the correlation plot of AGF experimental yields with the computed activation barriers of the rate-limiting step AG-ts3, in the presence and absence of AAEMs, respectively. The activation enthalpies of all the steps during the formation of AGF i.e., AG-ts1, AG-ts2 and AG-ts3; in the presence and absence of metal ions are listed in Table S2 of the supporting information.

The complexation of Mg(II) ions lowers the activation barriers of the first two steps i.e.,$(\mathbf{1}) \rightarrow (\mathbf{2})$ and $(\mathbf{2}) \rightarrow (\mathbf{3})$ to 40.0 and 34.8 kcal.mol^{-1}, respectively for AG-ts1 and AG-ts2. Similarly, the complexation of Ca(II) ions also decreases the activation barriers of AG-ts1 and AG-ts2 to 40.7 and 34.3 kcal.mol^{-1}, respectively. On the other hand, Mg(II) increases the activation enthalpy of the rate-limiting step i.e., $(\mathbf{3}) \rightarrow (\mathbf{4})$ to 61.9 kcal.mol^{-1}, while complexation with Ca(II) ion results in an activation barrier of 56.7 kcal.mol^{-1}. Furthermore, Na(I) and K(I) ions complex with AG-ts1 and AG-ts2 and result in barriers of 43 - 44 and 35 - 36 kcal.mol^{-1}, respectively, while the activation barrier of AG-ts3 decreases to 45.4 and 44.7 kcal.mol^{-1}, respectively, compared to 54.7 kcal.mol^{-1} for metal-free glucose. In summary, the trend in activation enthalpies of the rate-limiting step for AGF formation is as follows: Mg(II) > Ca(II) > K(I) > Na(I)/glucose, which, in turn, corresponds to the variation in AGF yield i.e., highest for Na(I)/glucose and the least is for Mg(II)/glucose.

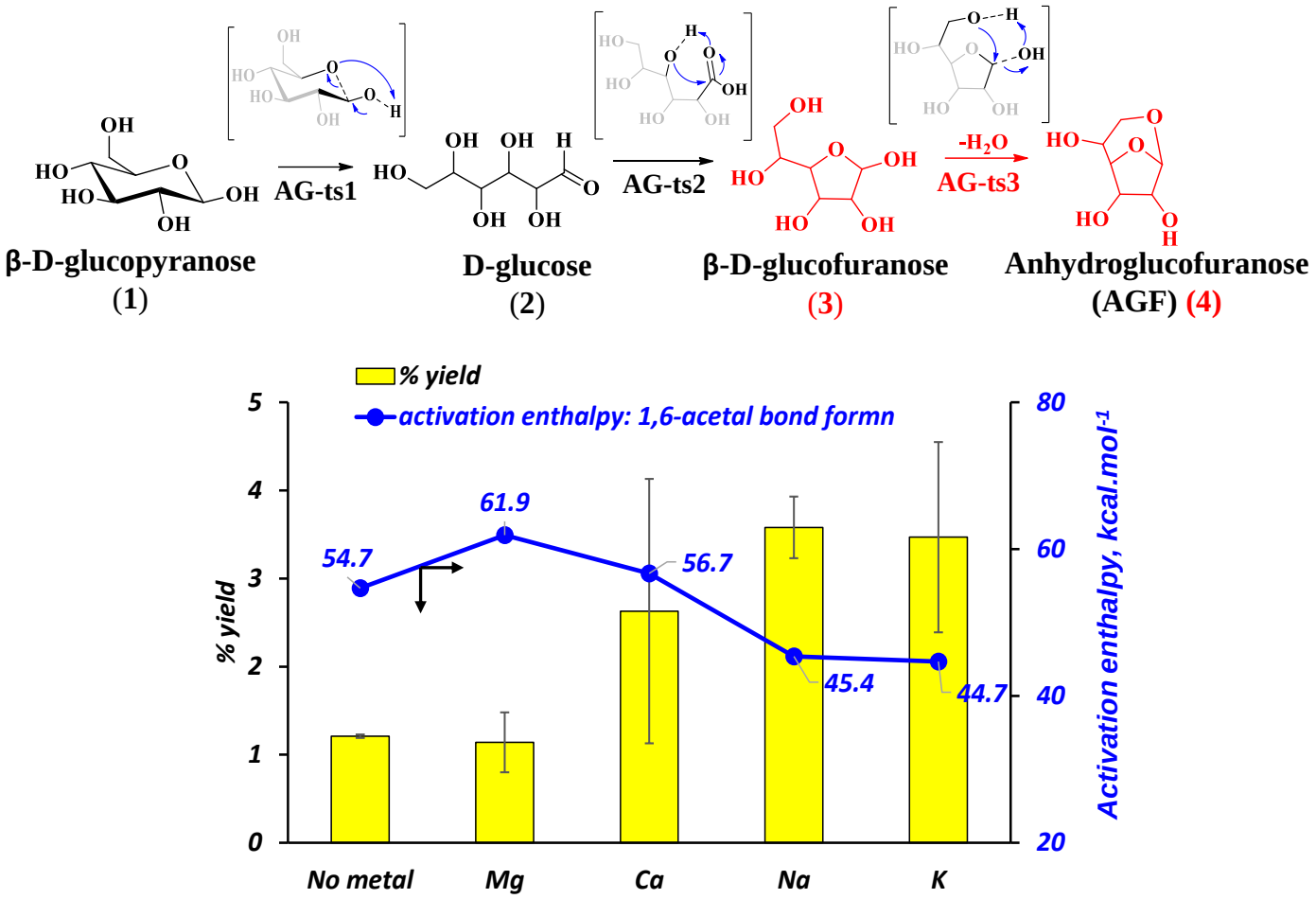

Figure 6: Correlation plot of the change in activation enthalpies of the rate-limiting step i.e., 1,6-acetal bond formation (shown in red in the reaction mechanism), in the presence and absence of alkali- and alkaline-earth metals with the change in 1,6-anhydroglucofuranose (AGF) experimental yields. The yield of AGF is expressed as %C basis. The blue arrows in the molecular structures show the electron flow during the reaction. Transition states of the reactions are illustrated above the arrow (in brackets), where the atoms not taking part in the reaction are faded.

View Article Online
DOI: 10.1039/C9CY00005D

4.4.2: *Formation of ADGH*

ADGH is categorized as a pyran. The experimental results of glucose pyrolysis show that in the absence of metal ions, ADGH yield is higher than that of metal-complexed glucose thin-film samples. ADGH formation from β-D-glucopyranose (**1**) takes place by the loss of a water molecule, i.e., O_1H and H_2 atoms generating 1,2-anhydroglucopyranose (**5**), which further undergoes dehydration and tautomerization forming ADGH (**7**). The activation barriers of the aforementioned three steps are labelled as AD-ts1, AD-ts2 and AD-ts3. In AD-ts1, the leaving group O_1H is stabilized by H from O_6H group. This results in elongation of O_6H bond distance to 1.06 Å. On the other hand, no intramolecular H-bonding is present with O_4H group and H_9 atoms of AD-ts2. In AD-ts3, tautomerization of the enol group at C_3 forms a four-membered cyclic transition state generating ADGH. In the absence of the metal ion, the activation enthalpies of AD-ts1, AD-ts2 and AD-ts3 are 60.2, 69.9 and 50.3 kcal.mol^{-1}, respectively. These activation barrier values are in agreement with the barriers reported by Hu et al. for ADGH formation [20].

The intermediate 1,2-anhydroglucopyranose can also undergo isomerization generating levoglucosan (LGA) [41]. Additionally, 1,2-anhydroglucopyranose can polymerize[22, 41] or react with other components, and can initialize char formation. The TS for 1,2-anhydroglucopyranose (**5**) to LGA (**8**) isomerisation i.e., Ch-tsR has an activation enthalpy of 53.3 kcal.mol^{-1}, while the reverse reaction i.e., LGA to 1,2-anhyglucopyranose, Ch-tsF, has an activation enthalpy of 61.0 kcal.mol^{-1}. Additionally, the condensation reaction of 1,2-anhydroglucopyranose with a reaction intermediate/ product of pyrolysis, in this case furfural, involves nucleophilic addition of 1,2-anhydroglucopyranose to carbonyl 'C' of furfural. The TS, Ch-ts1, has an activation barrier of 79.6 kcal.mol^{-1} in the absence of the metal ion. Thus, in the absence of the metal ion, the formation of ADGH is kinetically favorable as the activation enthalpies i.e., Ch-tsF and AD-ts2, for the generation and conversion of 1,2-anhydroglucopyranose (**5**), an important intermediate during ADGH formation, are lower than the other two competing reactions. Figure 7 shows the reaction scheme and the correlation plot of ADGH yields in the presence and absence of metal ions with the activation enthalpies of 1,2-anhydroglucopyranose to LGA isomerization, rate-limiting step i.e., AD-ts2 in ADGH formation and the reaction of 1,2-anhydroglucopyranose, i.e., Ch-ts1, to form char.

In Mg(II)/glucose, unlike H_6 bonding to the leaving group O_1H, intramolecular H-bonding between H_4 and O_6 exists due to the coordination of Mg(II) ions with O_3 and O_4 atoms in AD-ts1, which increases the activation enthalpy of AD-ts1 to 70.9 kcal.mol^{-1}. In the TS of the second step, AD-ts2, Mg(II) ions bind to the leaving O_4H group, facilitating the loss of water and lowers the activation enthalpy to 56.9 kcal.mol^{-1}. On the other hand in AD-ts3, Mg(II) ions coordinate with oxygen atom of the enol group at C_3 and increases the activation barrier to 56.1 kcal.mol^{-1}. Moreover, the coordination of Mg(II) ion with O_6 atom of 1,2-anhydroglucopyranose decreases the activation enthalpy to 33.0 kcal.mol^{-1} for the isomerization of 1,2-anhydroglucopyranose to LGA, while the activation barrier for the reverse reaction, Ch-tsF, increases to 76.9 kcal.mol^{-1} due to the coordination of Mg(II) ions with O_3 and O_4 in

Ch-tsF. The subsequent reaction of 1,2-anhydroglucopyranose (**5**) with furfural (**19**) resulting in char formation is not catalyzed by Mg(II) ions, thus resulting in an activation barrier of 80.9 kcal.mol^{-1}. Thus, the effect of Mg(II) ions on ADGH yield is anti-catalytic, as complexation of Mg(II) ion with 1,2-anhydroglucopyranose intermediate (**5**) favors isomerization to LGA over the other three competing reactions.

The coordination of Ca(II) ion with electron rich O-atoms in AD-ts1, AD-ts2 and AD-ts3 is similar to that exhibited by Mg(II) ion. The activation enthalpies of Ca(II) coordinated AD-ts1, AD-ts2 and AD-ts3 are 72.3, 69.4 and 53.5 kcal.mol^{-1}, respectively. During 1,2-anhydroglucopyranose to LGA isomerization, Ca(II) binds to O_3 and O_6 atoms in Ch-tsR and results in an activation enthalpy of 33.5 kcal.mol^{-1}, whereas in the TS of the reverse reaction i.e., Ch-tsF, Ca(II) ion coordinates with O_3 and O_4 atoms and results in an activation enthalpy of 69.4 kcal.mol^{-1}. In addition to this, during the reaction of 1,2-anhydroglucopyranose (**5**) with furfural (**19**), Ca(II) ion binds to the aldehydic oxygen of the furfural moiety and destabilizes Ch-ts1, resulting in the activation enthalpy of 83.8 kcal.mol^{-1}. Therefore, on comparing the activation enthalpies of the four parallel reactions taking place during ADGH formation, presence of Ca(II) ion kinetically favors conversion of intermediate 1,2-anhydroglucopyranose to LGA and hence the yield of ADGH is low.

However, in the presence of Na(I) and K(I) ions, the activation enthalpies of Na(I)/AD-ts1, Na(I)/AD-ts2 and Na(I)/AD-ts3 are 57.1, 73.0 and 51.9 kcal.mol^{-1}, respectively, while 57.5, 73.5 and 53.5 kcal.mol^{-1} are shown by K(I) assisted TSs. The enthalpic barrier of AD-ts1 corroborates with the reported activation energy value of 59.0 kcal.mol^{-1} for 1,2-dehydration in Na(I)/glucopyranose[25]. In AD-ts1, AD-ts2 and AD-ts3 TSs, the O-atoms coordinating with Na(I) and K(I) ions are similar. In AD-ts1, the alkali ion coordinates with O_1H and O_6H atoms, which slightly increases intramolecular H_6--O_1 bond distance to 1.45 Å. In alkali ion complexed AD-ts2, the univalent ions coordinate with O_4 and O_6 atoms, which, in turn, lowers the affinity of the leaving group O_4H to abstract the neighbouring H-atom and increases the activation enthalpy compared to metal-free AD-ts2. In AD-ts3, the alkali ion coordinates to the enolic O-atom of the 4-membered cyclic TS. The intermediate 1,2-anhydroglucopyranose (**5**) can isomerize to LGA (**8**) and vice versa. The enthalpic barrier of (**5**) → (**8**) isomerization, Ch-tsR, has activation enthalpies of 48.2 and 50.2 kcal.mol^{-1}, while the TS of the reverse reaction (**8**) → (**5**), Ch-tsF, has enthalpic barrier of 60.0 and 62.1 kcal.mol^{-1}, for Na(I) and K(I) ions, respectively. Further, complexation of Na(I) and K(I) ions with Ch-ts1assists in the coupling reaction of 1,2-anhydroglucopyranose (**5**) with furfural (**19**) initializing char formation and results in activation barrier values of 76.3 and 72.8 kcal.mol^{-1}, respectively.

Thus, by comparing the activation enthalpy values of AD-ts2, Ch-tsR, Ch-tsF and Ch-ts1, it can be seen that there are significant differences in the enthalpic barriers with and without AAEM ions. While the difference in the activation energies of these four parallel reactions is only about 7-10 kcal.mol^{-1} in the presence and absence of Na(I) and K(I) ions, about 25-30 kcal.mol^{-1} difference exists when Mg(II) and

View Article Online
DOI: 10.1039/C9CY00005D

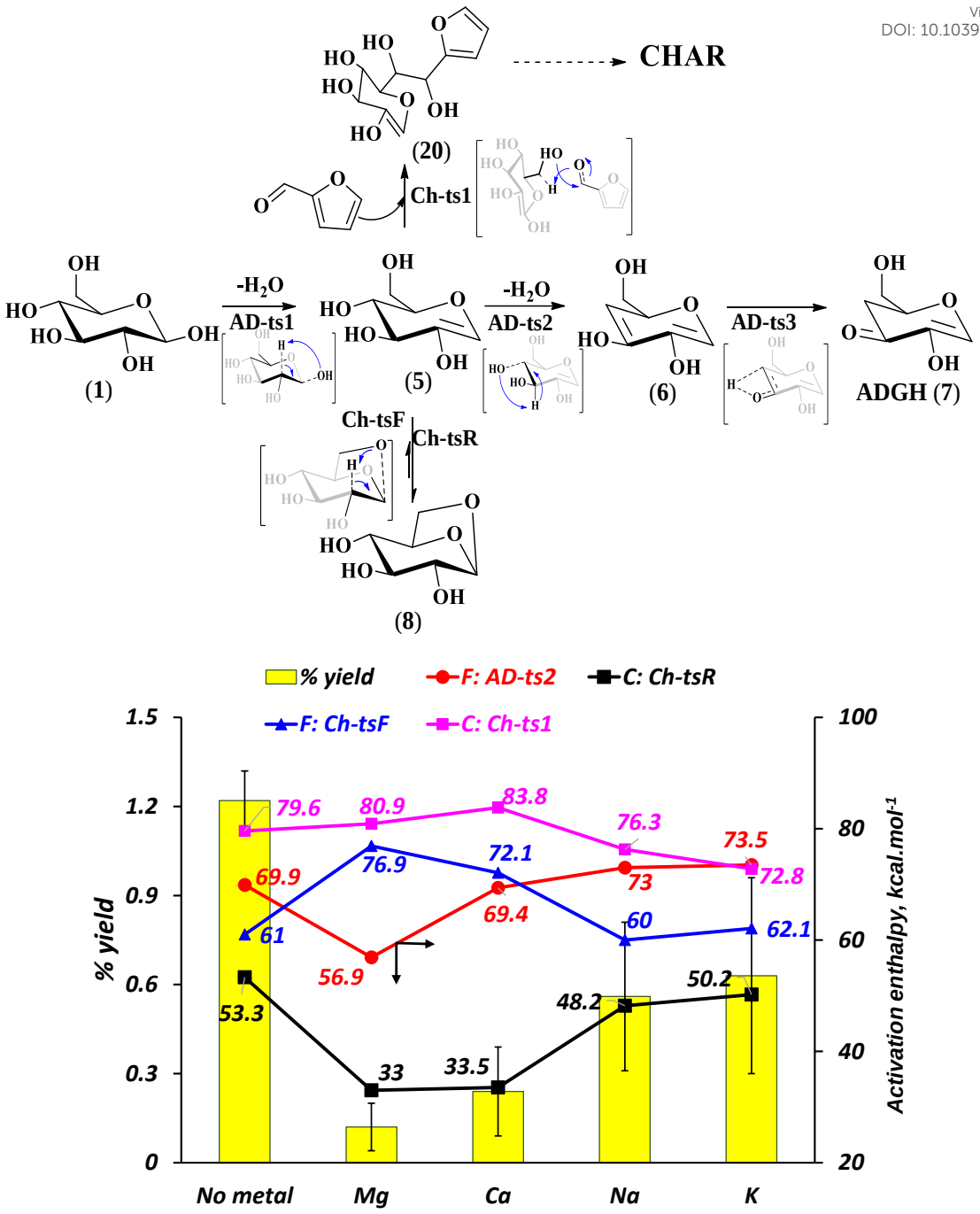

Figure 7: Reaction scheme and correlation plot of 1,5-anhydro-4-deoxy-D-glycerohex-1-en-3-ulose (ADGH) yield with the activation enthalpies of four competing reactions affecting ADGH formation in the presence and absence of alkali- and alkaline-earth metal ions. The yield of ADGH in the correlation plot is expressed as %C basis. The dotted arrow in the reaction scheme indicates secondary reactions. The labels of the transition states e.g. AD-ts1, are written on the reaction arrow. The labels F:AD-ts2 and F:Ch-tsF indicate the reactions that form ADGH/ its intermediate 1,2-anhydroglucopyranose, while C:Ch-ts1 and C:Ch-tsR indicate the reactions that convert the reaction intermediate of ADGH. The blue arrows in the molecular structures show the electron flow during the reaction. Transition states of the reactions are illustrated above the arrow (in brackets), where the atoms not taking part in the reaction are faded.

View Article Online
DOI: 10.1039/C9CY00005D

Ca(II) ions are present. These results explain the experimentally observed trend in ADGH yield, where the presence of metal ions effectively does not kinetically favour ADGH formation.

4.4.3: *Formation of Levoglucosan (LGA) and the subsequent conversion of LGA to Levoglucosenone (LGO)*

LGA is one of the predominant anhydrosugars formed during glucose pyrolysis.[35] The most common reaction pathway for LGA (**8**) formation is from β-D-glucopyranose (**1**), which involves loss of water i.e., -O_1H and H from O_6 followed by ring closure of O_6 at C_1 in a concerted manner.[23] The second reaction pathway for LGA formation involves isomerization of 1,2-anhydroglucopyranose (**5**). In addition to this, LGA, being unstable, can convert back to 1,2-anhydroglucopyranose (**5**) or even undergo two successive dehydrations and tautomerization generating LGO (**11**). Figures 8 [**A**] and 8 [**B**] show the reaction schemes and the correlation plot of LGA yield with the activation enthalpies of all four competing reactions affecting LGA formation in the presence and absence of AAEM ions.

In the absence of the metal ion, the TS for LGA formation from β-D-glucopyranose (**1**), LG-ts, shows that O_6 is stabilized by H-bonding with H of HO_3 group[23], as evident by the elongation of O_3-H_3 bond distance from 0.98 Å in the ground state of β-D-glucopyranose to 1.02 Å in LG-ts. The activation barrier for LGA formation from β-D-glucopyranose, LG-ts, is 47.2 kcal.mol^{-1}. 1,2-anhydroglucopyranose (**5**), generated as an intermediate during ADGH formation, can isomerize to LGA. The activation barrier of Ch-tsR is 53.3 kcal.mol^{-1}. For the conversion of LGA to LGO, the activation enthalpies of the three reaction steps i.e., LO-ts1, LO-ts2 and LO-ts3 are 71.5, 57.3 and 51.6 kcal.mol^{-1}, respectively. Of the three reaction steps in LGO formation, the first step of water loss i.e., LO-ts1, has the highest activation barrier and is the rate-limiting step in LGO formation. Furthermore, the TS for LGA to 1,2-anhydroglucopyranose conversion, Ch-tsF, results in an activation barrier of 61.0 kcal.mol^{-1}. Thus, in the absence of the metal ion, LGA is obtained in relatively high yield, because the activation enthalpies of the reactions forming LGA with TSs Ch-tsR and LG-ts are 5-15 kcal.mol^{-1} lower than the activation enthalpies of the reactions that convert LGA to other products, i.e., LO-ts1 and Ch-tsF.

In LG-ts, Mg(II) ions coordinate with O_1 and O_2 atoms. However, no H-bonding between H_3 and O_6 is observed in Mg(II)/LG-ts, unlike the TS in the absence of the metal. The activation barrier for LG-ts in the presence of Mg(II) ions is 48.2 kcal.mol^{-1}, which is comparable to the activation enthalpy of metal-free TS i.e., 47.2 kcal.mol^{-1}. On the other hand, the activation barrier of 1,2-anhydroglucopyranose (**5**) conversion to LGA, Ch-tsR, decreases to 33.0 kcal.mol^{-1}, as compared to 53.3 kcal.mol^{-1} in the metal-free reaction. In Ch-tsR, Mg(II) ions bind to O_6 atom facilitating ring closure and shortens the O_6-C_1 bond distance to 2.88 Å compared to 2.92 Å in metal-free TS. Further, Mg(II) ion coordinates with O_3 and O_4 atoms during LGA to 1,2-anhydroglucopyranose reaction and results in an activation enthalpy of 76.9 kcal.mol^{-1} for Ch-tsF. Next, binding of Mg(II) ions with O_2, O_4 and O_5 atoms in LO-ts1 results in activation enthalpy of 70.6 kcal.mol^{-1} which is similar to that of metal-free TS i.e., 71.5 kcal.mol^{-1}.

View Article Online
DOI: 10.1039/C9CY00005D

In LO-ts2, Mg(II) ions complex with O-atom of the enol group and increases the activation barrier to 66.3 kcal.mol^{-1}. Mg(II) ions coordinate with the leaving OH group i.e., O_4H in LO-ts3, which, in turn, increases the activation barrier to 55.2 kcal.mol^{-1}.

In the presence of Ca(II) ions, the metal ion binds to O_2 and O_4 atoms, with H_3 atom weakly bonded to O_6 in LG-ts. The activation barrier for LGA formation from (**1**) in the presence of Ca(II) ion is 52.0 kcal.mol^{-1}. The competing reaction of LGA (**8**) formation from 1,2-anhydroglucopyranose (**5**) is kinetically favorable as the activation barrier of Ch-tsR is 33.5 kcal.mol^{-1}. In Ch-tsR, Ca(II) ion binds to O_6 atom of (**5**). Further, the conversion of LGA (**8**) to 1,2-anhydroglucopyranose (**5**) in the presence of Ca(II) ions results in an activation barrier of 72.1 kcal.mol^{-1}, where Ca(II) ions complex with O_3 and O_4 atoms in Ch-tsF. In addition to this, the activation barrier of LO-ts1, which is also the rate-determining step in LGA to LGO reaction pathway, has an activation barrier of 72.1 kcal.mol^{-1}, while the subsequent steps i.e., LO-ts2 and LO-ts3 have activation enthalpies of 63.5 and 49.9 kcal.mol^{-1}. The oxygen binding sites for Ca(II) ions in LO-ts1, LO-ts2 and LO-ts3 are similar to that preferred by Mg(II) ions.

The coordination of Na(I) and K(I) ions in LG-ts is preferred with O_3 atom. Coordination of alkali ions at O_3 result in slight elongation of the interatomic distances between O_6, C_1 and O_1 atoms i.e., O_6-C_1 = 2.57-2.59 Å; O_1-C_1 = 2.80-2.82 Å; O_6-H_6 = 1.65-1.67 Å in Na(I) and K(I) complexed LG-ts compared to 2.62, 2.77 and 1.60 Å in the absence of the metal ion. However, the activation barrier values i.e., 47.0 and 48.2 kcal.mol^{-1} respectively, for Na(I) and K(I) assisted LG-ts, are similar to metal-free glucopyranose. Na(I) and K(I) binding to O_6 atom of 1,2-anhydroglucopyranose (**5**) in Ch-tsR decreases the activation enthalpies to 48.2 and 50.2 kcal.mol^{-1}, respectively, compared to 53.3 kcal.mol^{-1} in metal-free TS. On the other hand, the activation enthalpies for the ring opening of LGA to 1,2-anhydroglucopyranose in the presence of Na(I) and K(I) ions have activation enthalpies of 60.0 and 62.1 kcal.mol^{-1}, respectively, which are similar to metal-free Ch-tsF of 61.0 kcal.mol^{-1}. In Ch-tsF, Na(I) and K(I) ions bind to O_6 atom of LGA, interatomic distance is metal(I)-O_6 = 2.17 and 2.47 Å, respectively. The metal ion and O_6 bond distance in Ch-tsF is 0.03-0.05 Å higher than Ch-tsR, while the interatomic distances between H_2, O_6 and C_1 are similar in Ch-tsF and Ch-tsR. Thus, the difference in the activation barriers of Ch-tsF and Ch-tsR is attributed to the higher stability of the metal(I)-LGA complex compared to metal(I)-1,2-anhydroglucopyranose complex. In addition to this, the activation barriers of LO-ts1, LO-ts2 and LO-ts3 during LGO formation are 75.4, 61.0 and 49.7 kcal.mol^{-1} in presence of Na(I) ions, while 74.4, 60.2 and 50.9 kcal.mol^{-1}, respectively for K(I) assisted. In LO-ts1, Na(I) and K(I) ions bind to O_2, O_4 and O_5 atoms, while, the metal ions coordinate with O-atom of the enol group in LO-ts2 and with O_4 atom in LO-ts3.

In summary, the presence of Mg(II) and Ca(II) ions catalyzes the reaction steps for the formation of LGA, i.e., Ch-tsR and LG-ts, owing to activation enthalpies of 33.0, 48.2 and 33.5, 52.0 kcal.mol^{-1} for Mg(II) and Ca(II) catalyzed TSs, respectively. However, the activation barriers for Ch-tsR in the presence of Na(I) and K(I) increase by 15-17 kcal.mol^{-1}, compared to the activation enthalpies for

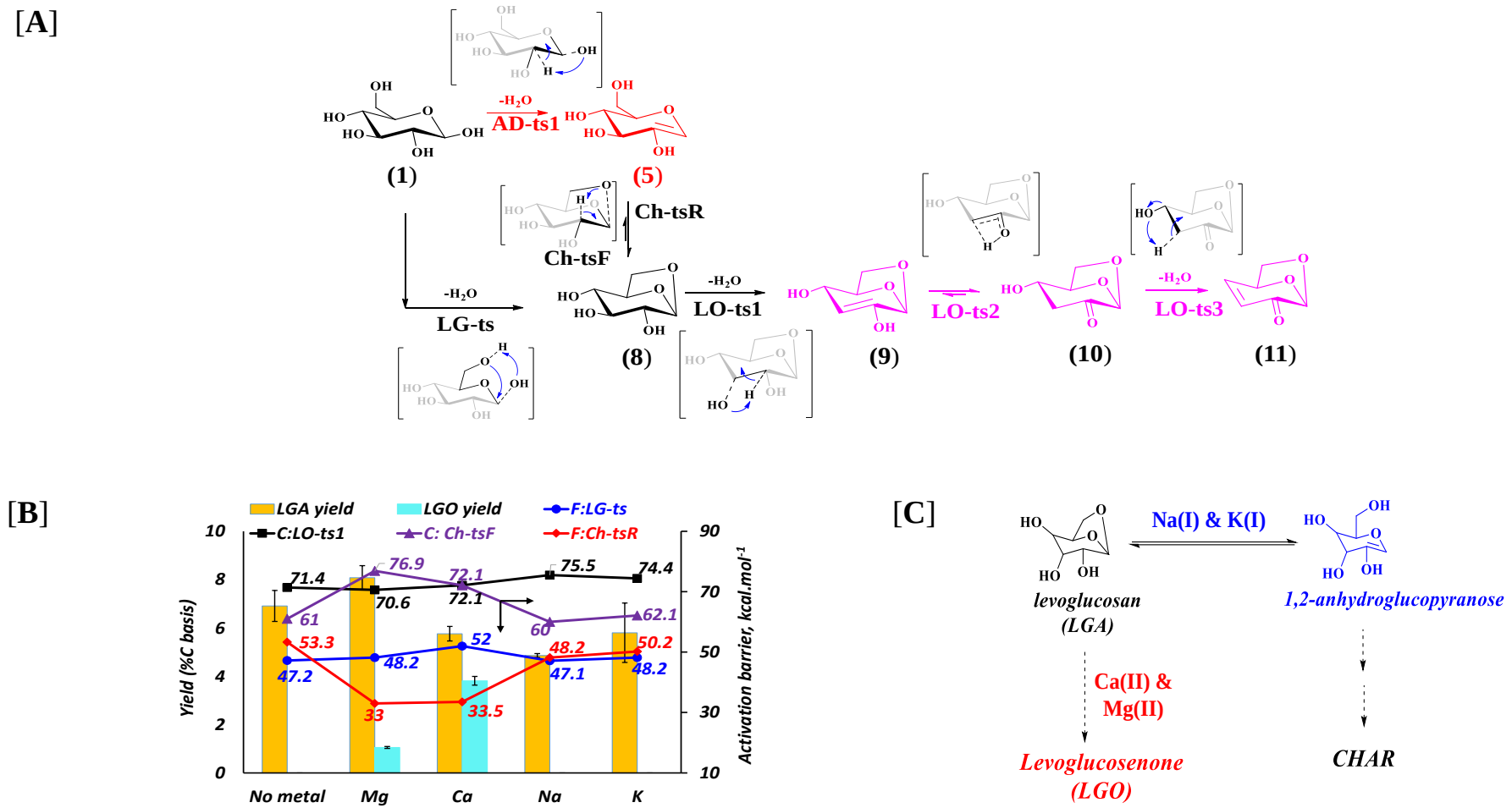

Figure 8: [**A**] and [**B**] Reaction scheme and correlation plot of levoglucosan (LGA) yield with the activation enthalpies of four competing reactions affecting LGA formation in the presence and absence of alkali and alkaline-earth metal ions. [**C**] Fate of LGA in the presence of alkali and alkaline-earth metal ions. The yield of LGA in the correlation plot is expressed as %C basis. The dotted arrows in [**C**] indicate the secondary reactions of the molecules. The labels of the transition states e.g. LG-ts, are written on the reaction arrow. The labels F:LG-ts and F:Ch-tsR indicate the reactions that form LGA, while C:Ch-tsF and C:LO-ts1 indicate the reactions that convert LGA. The blue arrows in the molecular structures show the electron flow during the reaction. Transition states of the reactions are illustrated above the arrow (in brackets), where the atoms not taking part in the reaction are faded.

Mg(II) and Ca(II) assisted reactions. On the other hand, Mg(II) and Ca(II) ions also catalyze the subsequent breakdown of LGA (**8**) to LGO (**11**) as these ions lower the activation barrier of LO-ts1, which is the rate-limiting step, but have an anti-catalytic effect on LGA conversion to 1,2-anhydroglucopyranose. Moreover, Na(I) and K(I) exhibit a reverse trend for LGA conversion reactions compared to Ca(II) and Mg(II) ions, i.e., Na(I) and K(I) ions have a neutral effect on LGA conversion to 1,2-anhydroglucopyranose, while the activation enthalpies to convert LGA to LGO increases by 4-5 kcal.mol^{-1}. Therefore, in the absence of metal ions and in the presence of alkali ions LGA yield is lowered as 1,2-anhydroglucopyranose formation is favoured, which further reacts to give char.[41] Conversely, the presence of Ca(II) and Mg(II) ions kinetically favors conversion of 1,2-anhydroglucopyranose to LGA, which, in turn, reacts to form LGO. Thus, the fate of LGA is decided by its chemical surroundings and the relative reaction rates of all these reaction pathways influence the experimental yield of LGA. Figure 8 [**C**] summarizes the fate of LGA in the presence of AAEM ions.

4.4.4: *5-hydroxymethylfurfural (5-HMF) formation and its conversion to furfural*

5-HMF is an important product obtained during biomass pyrolysis.[24] However, experimental results show that lower yield (<1%) of 5-HMF is obtained in metal-free and AAEM-complexed glucose pyrolysis. Figure 9 shows the reaction pathway for 5-HMF formation from β-D-glucopyranose (**1**) as well as the correlation of the experimental yield of 5-HMF with the activation barriers for the formation and conversion of 5-HMF. 5-HMF formation involves a series of ring opening and dehydration reactions of β-D-glucopyranose (**1**). Two routes for keto-intermediate (**15**) formation are possible.[24] Route one involves D-fructose (**12**) as an intermediate (reaction arrows in black), while route two involves cyclization of D-glucose (**2**) with water loss (reaction arrows shown in pink). Furthermore, the ketone intermediate (**15**) also exhibits two competing routes for 5-HMF formation depending upon the loss of first water molecule from 'C' alpha to the aldehydic side group (intermediate shown in red in the reaction scheme) or primary hydroxyl group.

The activation barriers for glucopyranose ring opening (AG-ts1), isomerization of glucose to fructose (HM-ts1), fructofuranose formation (HM-ts2) and dehydration (HM-ts3) followed by tautomerization (HM-ts4) are 45.4, 39.3, 29.5, 66.5, 58.9 kcal.mol^{-1}, respectively, while dehydrative cyclization of D-glucose (**2**) to ketone-intermediate (**15**) (HM-ts5) exhibits an activation barrier of 78.1 kcal.mol^{-1}. These activation enthalpies suggest that the formation of ketone intermediate via the fructose intermediate is kinetically favorable. Once the ketone intermediate is formed, loss of a water molecule can occur from 'C' alpha to alcoholic side group, HM-ts6, or from 'C' alpha to aldehydic side group, HM-ts7, resulting in enthalpic barriers of 73.7 and 56.7 kcal.mol^{-1}, respectively. The enthalpic barrier of HM-ts7 is about 18 kcal.mol^{-1} lower than that of HM-ts6, because HM-ts7 is stabilized by conjugation with the neighbouring aldehydic group. Loss of another water molecule from intermediates (**16**) and (**17**) results in the formation of 5-HMF. The activation enthalpies of TSs, HM-ts8 and HM-ts9, are 51.1 and 55.2 kcal.mol^{-1}, respectively. The above results are in corroboration with the findings reported by Mayes et

View Article Online
DOI: 10.1039/C9CY00005D

al.[24] for 5-HMF formation. 5-HMF once formed, can undergo subsequent deformylation generating furfural (FU-ts), thus resulting in an activation barrier of 78.4 kcal.mol^{-1}. Analysis of the activation barriers of metal-free glucose shows that 5-HMF formation via the fructose intermediate is the kinetically preferred route and the dehydration of β-D-fructofuranose to enol i.e., HM-ts3 is the rate-determining step.

The activation enthalpies of AG-ts1 and HM-ts1 to HM-ts4 for Mg(II)/glucose complex are 39.3, 25.9, 24.3, 38.3 and 57.1 kcal.mol^{-1}, while in the presence of Ca(II) ions the activation enthalpies are 39.5, 29.2, 36.7, 47.9 and 66.0 kcal.mol^{-1}, respectively. The complexation of divalent Mg(II) and Ca(II) ions in the TSs, HM-ts1 to HM-ts4, lower the activation enthalpies by 5-15 kcal.mol^{-1} when compared to metal-free TSs. Furthermore, the activation enthalpies for the conversion of Mg(II) complexed ketone intermediate (**15**) to HMF via loss of water from the hydroxyl side group, HM-ts6 and HM-ts8 are 63.1 and 42.9 kcal.mol^{-1}, while the loss of water from aldehydic side group in (**15**), HM-ts7 and HM-ts9, are 44.9, 64.5 kcal.mol^{-1}, respectively. For Ca(II) assisted HM-ts6 and HM-ts8, the activation barriers are 64.5 and 44.3 kcal.mol^{-1}, while HM-ts7 and HM-ts9 have activation enthalpy values of 73.7, 63.1 kcal.mol^{-1}, respectively. It can be seen that two successive dehydrations of the ketone intermediate (**15**) are preferred from the hydroxyl side chain for Ca(II) coordinated intermediate (**15**), while Mg(II) ions kinetically favor loss of first water molecule from the aldehydic side group. This can be attributed to the fact that H of CHO side group forms a weak H-bond with the hydroxyl group of αC (bond distance 2.68 Å) in Ca(II) complexed HM-ts7, while this bond distance is >3.5 Å for Mg(II) complexed TS. The presence of H-bonding in Ca(II)/HM-ts7 lowers the affinity of the hydroxyl group to abstract the H atom from the neighbouring C-atom in case of Ca(II), thus increasing the activation barrier to 73.7 kcal.mol^{-1} as compared to 44.9 kcal.mol^{-1} for Mg(II). Furthermore, the activation barriers for the conversion of HMF to furfural, FU-ts, are 60.1 and 65.6 kcal.mol^{-1}, respectively for Mg(II) and Ca(II) assisted TSs. On comparing the activation barrier of the rate-determining step for 5-HMF formation i.e., HM-ts3 with that of its conversion reaction, FU-ts, it can be seen that the delta between HM-ts3 and FU-ts activation barriers is about 6 kcal.mol^{-1} for metal-free conditions, while presence of Mg(II) slightly lowers the delta of activation barriers and Ca(II) ions have a neutral effect. Further, the slight difference in the activation enthalpies for the formation and conversion reaction, with the conversion reaction being kinetically favorable for Mg(II) and Ca(II), explains the lower yield of HMF in the presence of divalent ions.

In the presence of Na(I) and K(I) ions, the activation enthalpy values of AG-ts1 and HM-ts1 to HM-ts4 are 42.5, 31.9, 31.5, 62.9 and 62.8 kcal.mol^{-1} for Na(I)/glucose complex, while in the presence of K(I) ions the activation enthalpies are 41.8, 38.2, 30.7, 64.9 and 63.1 kcal.mol^{-1}, respectively. The complexation of Na(I) and K(I) ions in the TSs AG-ts, HM-ts1 to ts4 slightly lower the activation enthalpies by 3-5 kcal.mol^{-1} when compared to metal-free TSs. Similar to the case Mg(II) ions, the complexation of Na(I) and K(I) ions with the ketone intermediate (**15**) also kinetically favors loss of water from the aldehydic side. The activation enthalpies of Na(I) complexed HM-ts6 and HMts8 are

View Article Online
DOI: 10.1039/C9CY00005D

68.7 and 47.5 kcal.mol^{-1}, while 51.7 and 62.5 kcal.mol^{-1}, respectively for HM-ts7 and HM-ts9. On the other hand, the activation enthalpies of K(I) complexed HM-ts6 and HMts8 are 68.0 and 46.9 kcal.mol^{-1}, while 51.4 and 58.0 kcal.mol^{-1}, respectively for HM-ts7 and HM-ts9. Moreover, the activation barriers for the conversion of HMF to furfural, FU-ts, are 74.5 and 76.4 kcal.mol^{-1} for Na(I) and K(I) assisted TSs, which are 2-4 kcal.mol^{-1} lower than metal-free FU-ts. In summary, the presence of Na(I) and K(I) ions have a neutral effect on conversion of HMF and thus the yield of HMF in presence of alkali ions is similar to that of metal-free glucose.

4.4.5: *Formation of furfural and the condensation reaction of furfural with 1,2-anhydroglucopyranose initiating char formation*

Figure 10 shows the correlation plot and the reaction scheme for furfural formation and its subsequent reaction with 1,2-anhydroglucopyranose which initiates char formation and correlates furfural yield with the activation barriers associated with TSs FU-ts and Ch-ts1.The experimental results show that furfural yield is maximum from Mg(II)/glucose thin-film samples, followed by Ca(II) ions and least is in metal-free glucose. The computed activation barrier for deformylation of 5-HMF[25], FU-ts, in the absence of metal ion is 78.4 kcal.mol^{-1}. As discussed in section 4.4.2, furfural can also undergo a coupling reaction with 1,2-anhydroglucopyranose intermediate resulting in the formation of an α,β-dihydroxy adduct (**20)**. The activation barrier for the above mentioned coupling reaction is 79.5 kcal.mol^{-1}, which is similar to that of FU-ts.

Complexation of Mg(II) ions with oxygen of the hydroxyl side group in FU-ts assists in C-C bond breaking and results in the activation enthalpy of 60.1 kcal.mol^{-1}, while the coupling reaction of furfural (**19**) with 1,2-anhydroglucopyranose (**5**) is decatalyzed by complexation of Mg(II) ions with O_3 and O_4 atoms of (**5**). The reaction $(\mathbf{19}) + (\mathbf{5}) \rightarrow (\mathbf{20})$ has an activation barrier of 80.9 kcal.mol^{-1}. Similarly, Ca(II) ion complexation also assists in furfural formation resulting in 65.6 kcal.mol^{-1} for Fu-ts, while the activation barrier of Ch-ts1 increases to 83.8 kcal.mol^{-1} when Ca(II) ions coordinate with O_6 and aldehydic oxygen of furfural.

Conversely, binding of Na(I) and K(I) ions with oxygen of the hydroxyl side group in HMF slightly lowers the activation enthalpies to 74.5 and 76.4 kcal.mol^{-1}, respectively compared to metal-free FU-ts, whereas the enthalpic barriers for Ch-ts1 are lowered by 3-6 kcal.mol^{-1}. To summarize, the presence of Na(I) and K(I) ions as well as in metal-free conditions, the formation of furfural and its subsequent conversion reaction compete with each other owing to similar activation enthalpies. Further, the activation enthalpies for FU-ts and Ch-ts1 are higher by 6-8 kcal.mol^{-1} compared to the enthalpic barriers of Na(I) and K(I) ions, which explains the lower yield of furfural in metal-free conditions compared to Na(I) and K(I) ions. In contrast, Mg(II) and Ca(II) complexed FU-ts result in activation barriers which are about 18-20 kcal.mol^{-1} lower than Ch-ts1 and hence the yield of furfural is high as compared to metal-free and alkali ion assisted furfural yields.

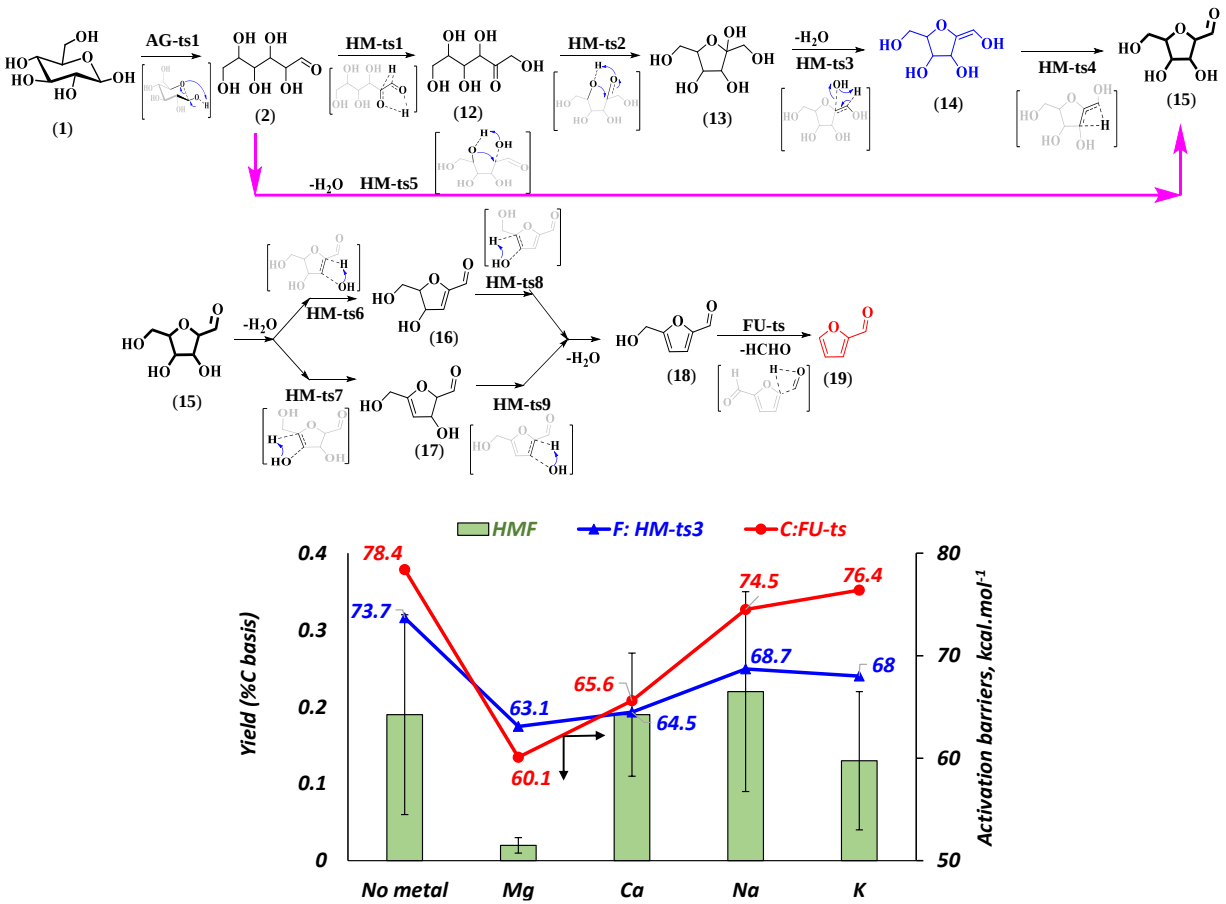

Figure 9: Reaction scheme and correlation plot of 5-hydroxymethylfurfural (5-HMF) yield with the activation enthalpies of two competing reactions affecting HMF formation in the presence and absence of alkali and alkaline-earth metal ions. The yield of HMF in the correlation plot is expressed as %C basis. The labels of the transition states e.g. AG-ts1, are written on the reaction arrow. The labels F:HM-ts3 and C:FU-ts indicate the reactions that form and convert HMF. The blue arrows in the molecular structures show the electron flow during the reaction. Transition states of the reactions are illustrated above the arrow (in brackets), where the atoms not taking part in the reaction are faded.

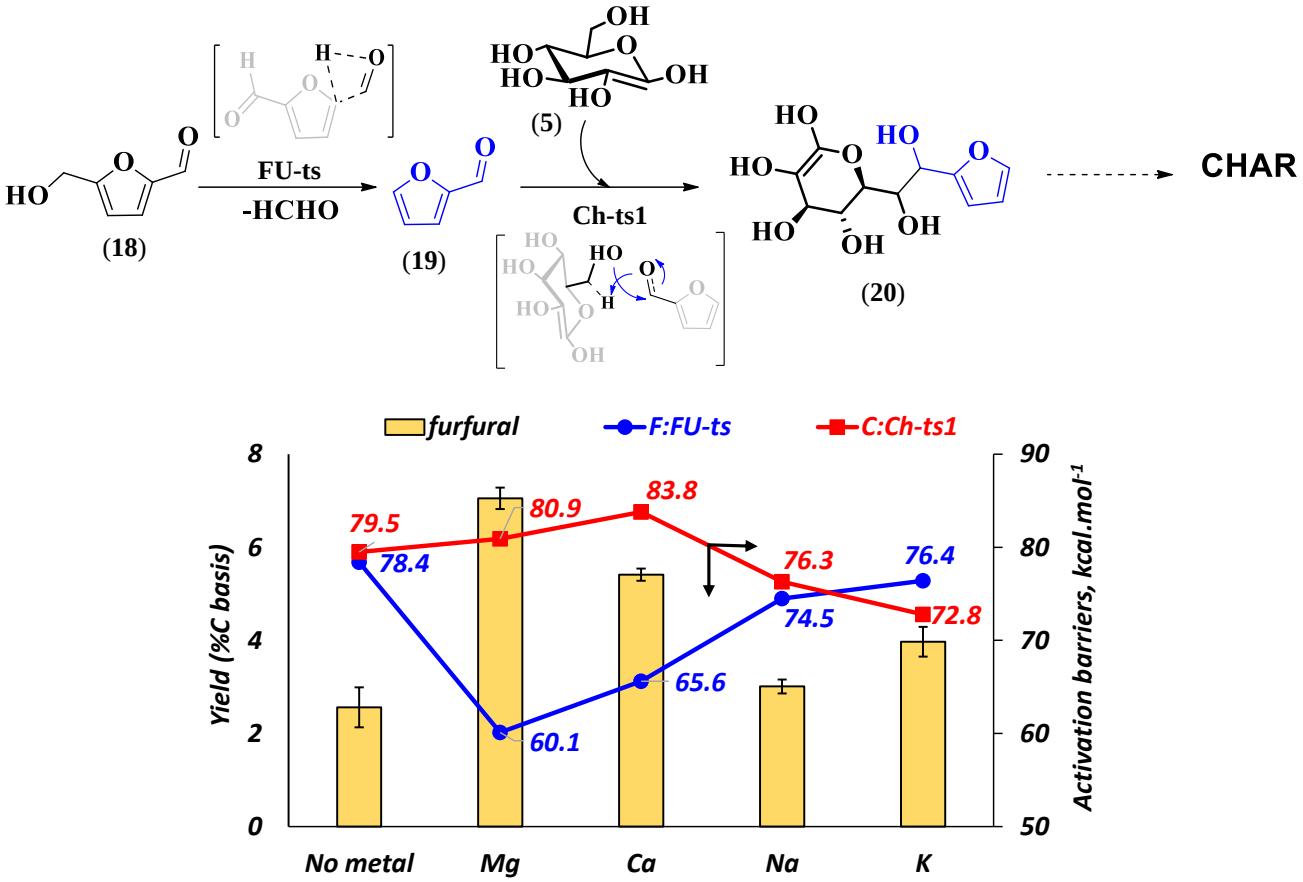

Figure 10: Reaction scheme and correlation plot of furfural yield with the activation enthalpies of two competing reactions affecting furfural formation in the presence and absence of alkali and alkaline-earth metal ions. The yield of furfural in the correlation plot is expressed as %C basis. The dotted arrows in the reaction scheme indicate the secondary reaction of intermediate (**20**). The labels of the transition states e.g. FU-ts, are written on the reaction arrow. The labels F:FU-ts, and C: Ch-ts1 indicate the reactions that form and convert furfural, respectively. The blue arrows in the molecular structures show the electron flow during the reaction. Transition states of the reactions are illustrated above the arrow (in brackets), where the atoms not taking part in the reaction are faded.

View Article Online
DOI: 10.1039/C9CY00005D

4.4.6: *Reaction Network for Char formation*

As discussed in section 4.1, Na(I) and K(I) complexed glucose pyrolysis under reaction-controlled regime increases the yield of char by 9-10 %, while Ca(II) and Mg(II) ions alter the yield of char by 2-3%, as compared to metal-free glucose. Char formation is a convoluted process and predominantly involves dehydration and bimolecular condensation reactions of C5 molecules and dehydrated volatile products/intermediates.[22] The relative change in the yield of pyrolysis products in the presence and absence of AAEM ions show that an increase in char yield results in the corresponding decrease of LGA and C5 molecules (in this case: 5-HMF and furfural) in the presence of Na(I) and K(I) ions, while a reverse trend is seen in the presence of Ca(II) and Mg(II) ions. Figure 11 shows the reaction pathway computed for char formation. Figure 12[**A**] compares the cumulative yield of LGA and C5 compounds with char yield and Fig. 12[**B**] shows the correlation plot of the difference in char yield with the activation enthalpies of ***a***) the reactions generating 1,2-anhydroglucopyranose (**5**) (AD-ts1 and Ch-tsR) and furfural (**19**) (FU-ts), ***b***) the rate-limiting step i.e., nucleophilic addition reaction of 1,2-anhydroglucopyranose with nucleophile Ch-ts1 and ***c***) the competitive reactions of (**5**) having TSs Ch-tsF and AD-ts2, in the presence and absence of alkali- and alkaline-earth metal ions.

As discussed in section 4.4.3, 1,2-anhydroglucopyranose (**5**) (generated from β-D-glucopyranose (**1**) or from isomerization of LGA (**8**)) can attack electron-deficient 'C' of C5 species (e.g. furfural or 5-HMF) by nucleophilic addition reaction to form an α,β-diol (Ch-int1). The Ch-int1 intermediate (**20**) then undergoes dehydration, forming two enol intermediates, namely Ch-int2G (**21**) and Ch-int2F (**22**) with TSs Ch-ts2G and Ch-ts2F. The next step involves tautomerization of the enol generating ketone intermediates i.e., Ch-int3G (**23**) and Ch-int3F (**24**). The ketone intermediates are highly reactive due to the presence of α-H atoms and hence can further react with a carbonyl intermediate or can undergo nucleophilic addition reaction with the primary hydroxyl group of an intermediate/product. We suggest that the ketone intermediates (**23**) and (**24**) can further undergo a series of secondary reactions in the pyrolysis condensed phase, thus contributing to char.

Further, the activation enthalpies of char formation are compared with competing reactions of (**5**), i.e., isomerization to LGA (Ch-tsR) and conversion to ADGH (AD-ts2). In Fig. 12[**B**], the difference between the yields of char for metal-assisted and metal-free conditions is plotted on the y-axis. This is because pyrolysis of glucopyranose is conducted at 200°C, which may leave behind certain amount of unconverted glucose along with char. Thus, to cancel out the presence of unconverted glucose, the yield of char for metal-free glucopyranose is subtracted from the char yield of metal-assisted glucose pyrolysis. As discussed in sections 4.4.2 and 4.4.5, the activation enthalpies for the formation of the two reactants, (**5**) and (**19**), in metal-free glucose are 60.2, 61.0 and 78.4 kcal.mol^{-1} for AD-ts1, Ch-tsF and FU-ts, respectively. In the absence of the metal ion, the two reactants (**5**) and (**19**) can react to form char and result in activation enthalpies of 79.5, 67.5, 66.1, 63.6, and 54.1 kcal.mol^{-1} for Ch-ts1, Ch-ts2G, Ch-ts2F, Ch-ts3G and Ch-ts3F, respectively. In addition to this, (**5**) can also convert back to LGA

View Article Online
DOI: 10.1039/C9CY00005D

or undergo loss of a water molecule generating intermediate (**6**). These two reactions, i.e., Ch-tsR and AD-ts2, have activation barriers of 53.3 and 69.9 kcal.mol^{-1}, respectively. On analyzing the activation barriers of all the competing reactions involved in the formation of char, it can be seen that the nucleophilic addition of 1,2-anhydroglucopyranose to C5 component furfural, i.e., Ch-ts1, is the rate-determining step.

In the presence of Mg(II) ions, the activation enthalpies for the formation of (**5**) and (**19**) are 82.5, 76.9 and 60.1 kcal.mol^{-1} for AD-ts1, Ch-tsF and FU-ts, respectively. Thus, coordination of Mg(II) ions decatalyzes 1,2-anhydroglucopyranose formation (AD-ts1, Ch-tsF), while Mg(II) ions have a catalytic effect on the formation of furfural (FU-ts) when compared to the activation barriers of metal-free TSs i.e., 60.2, 61.0 and 78.4 kcal.mol^{-1}. Subsequent reaction of 1,2-anhydroglucopyranose (**5**) to char results in an activation barrier of 80.9, 64.7, 67.4, 61.3 and 49.7 kcal.mol^{-1}, for Ch-ts1, Ch-ts2G, Ch-ts2F, Ch-ts3G and Ch-ts3F, respectively. However, reactant (**5**) can readily convert to LGA (Ch-tsR) or undergo dehydration and result in activation barriers of 33.0 and 56.9 kcal.mol^{-1}, respectively, for Ch-tsR and AD-ts2. The binding of Ca(II) ions in AD-ts1, Ch-tsF and FU-ts result in activation enthalpies of 77.9, 72.1 and 65.6 kcal.mol^{-1}, respectively. The presence of Ca(II) ions also decatalyzes 1,2-anhydroglucopyranose formation compared to metal-free TS, while Ca(II) ions have a catalytic effect on the formation of furfural. Subsequent reaction of 1,2-anhydroglucopyranose (**5**) with furfural (**19**) to char exhibits a barrier of 83.8 kcal.mol^{-1} (for TS Ch-ts1), which is about 5 kcal.mol^{-1} higher than metal-free Ch-ts1. The activation barriers for Ch-ts2G, Ch-ts2F, Ch-ts3G and Ch-ts3F are 62.5, 68.4, 62.8, and 52.7 kcal.mol^{-1}, respectively. But, subsequent reaction of (**5**) to LGA is kinetically favorable over the dehydration reaction generating ADGH. The activation enthalpies for Ch-tsR and AD-ts2 in the presence of Ca(II) ions are 33.5 and 69.4 kcal.mol^{-1}, respectively. On comparing the activation enthalpies of all the six reactions with the char yield for metal-free and divalent complexed TSs, char formation in the presence of Mg(II) and Ca(II) ions is kinetically unfavorable as (**5**) prefers to form LGA, owing to 30-40 kcal.mol^{-1} difference in the activation barrier values for divalent complexed Ch-ts1 and Ch-tsR. Hence, these DFT calculations explain the change (by 2-3%) in char yield for Mg(II)/glucose and Ca(II)/glucose, when compared to metal-free glucose.

On the other hand, the activation barriers for the formation of the (**5**) and (**19**) in Na(I)/glucose are 57.1, 62.1 and 74.5 kcal.mol^{-1} for AD-ts1, Ch-tsF and FU-ts, respectively. Thus, coordination of Na(I) ions lowers the activation enthalpies of 1,2-anhydroglucopyranose (AD-ts1, Ch-tsF) and furfural formation (FU-ts) by 1-3 kcal.mol^{-1}, compared to the activation barriers of metal-free TSs, which are 60.2, 61.0 and 78.4 kcal.mol^{-1}. The activation barriers for Na(I)-assisted Ch-ts1, Ch-ts2G, Ch-ts2F, Ch-ts3G and Ch-ts3F are 76.3, 66.8, 68.8, 63.3 and 53.6 kcal.mol^{-1}, respectively. However, (**5**) can also convert to LGA or undergo dehydration and result in activation barriers of 48.2 and 73.0 kcal.mol^{-1}, respectively in the presence of Na(I) ions. In addition to this, the binding of K(I) ions in AD-ts1, Ch-tsF and FU-ts result in activation enthalpies of 57.5, 50.2 and 76.4 kcal.mol^{-1}, respectively. The presence of K(II) ions too lower the activation enthalpies of 1,2-anhydroglucopyranose (AD-ts1, Ch-tsF) and furfural

View Article Online
DOI: 10.1039/C9CY00005D

formation (FU-ts) by 1-2 kcal.mol^{-1} compared to the activation barriers of metal-free TSs. Subsequent reaction of 1,2-anhydroglucopyranose (**5**) with furfural to form char exhibits the enthalpic barrier of 72.8 kcal.mol^{-1} (for Ch-ts1), which is about 6 kcal.mol^{-1} lower than metal-free Ch-ts1. The activation barriers for Ch-ts2G, Ch-ts2F, Ch-ts3G and Ch-ts3F are 66.5, 68.6, 63.2, and 53.7 kcal.mol^{-1}, respectively. But, subsequent reaction of (**5**) to LGA (Ch-tsR) and the dehydration reaction generating ADGH (AD-ts2) have activation barriers of 50.2 and 73.5 kcal.mol^{-1}, which are comparable to the activation enthalpies of char formation. Therefore, on comparing the activation enthalpies of all the six reactions with the char yield for metal-free and alkali metal complexed TSs, char formation in the presence of Na(I) and K(I) ions is kinetically favorable as (**5**) prefers to condense with furfural (**19**), owing to a slight difference in the activation barrier values of univalent complexed Ch-ts1 and metal-free Ch-ts1. Thus, the DFT calculations explain the increase in char yield for Na(I) and K(I)-complexed glucose by 9-10% when compared to metal-free glucose.

View Article Online
DOI: 10.1039/C9CY00005D

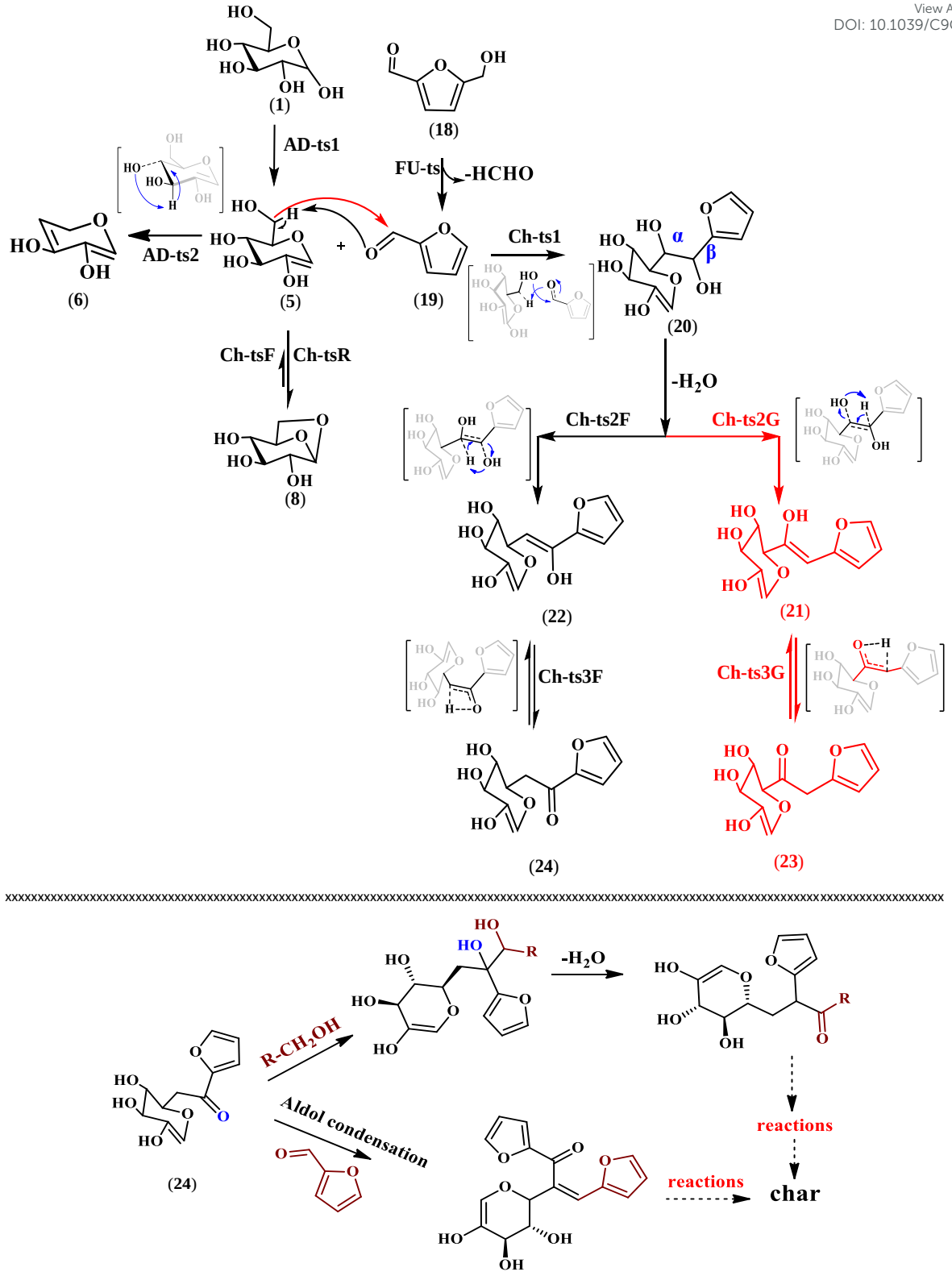

Figure 11: Coupling reaction of 1,2-anhydroglucopyranose (**5**) with a nucleophile (here furfural) resulting in C-C bond formation along with series of addition/dehydration reactions of Ch-int3F (**24**) giving char. The dotted arrows indicate secondary reactions of intermediates resulting in char formation. The blue arrows in the molecular structures show the electron flow during the reaction. Transition states of the reactions are illustrated above the arrow (in brackets), where the atoms not taking part in the reaction are faded.

View Article Online
DOI: 10.1039/C9CY00005D

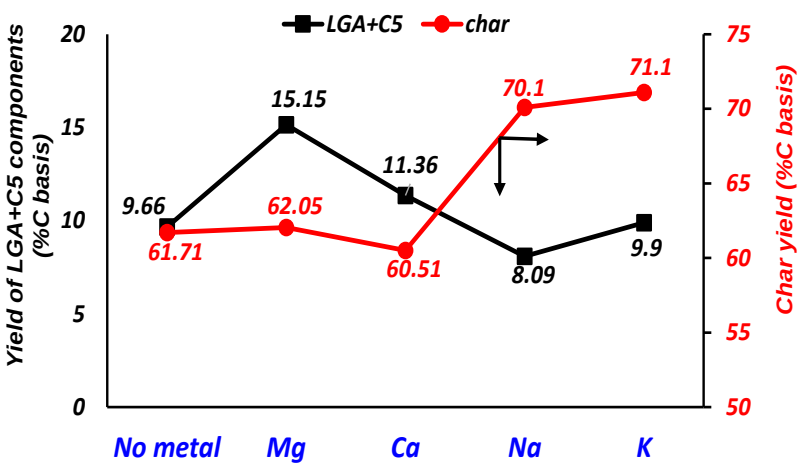

[A]

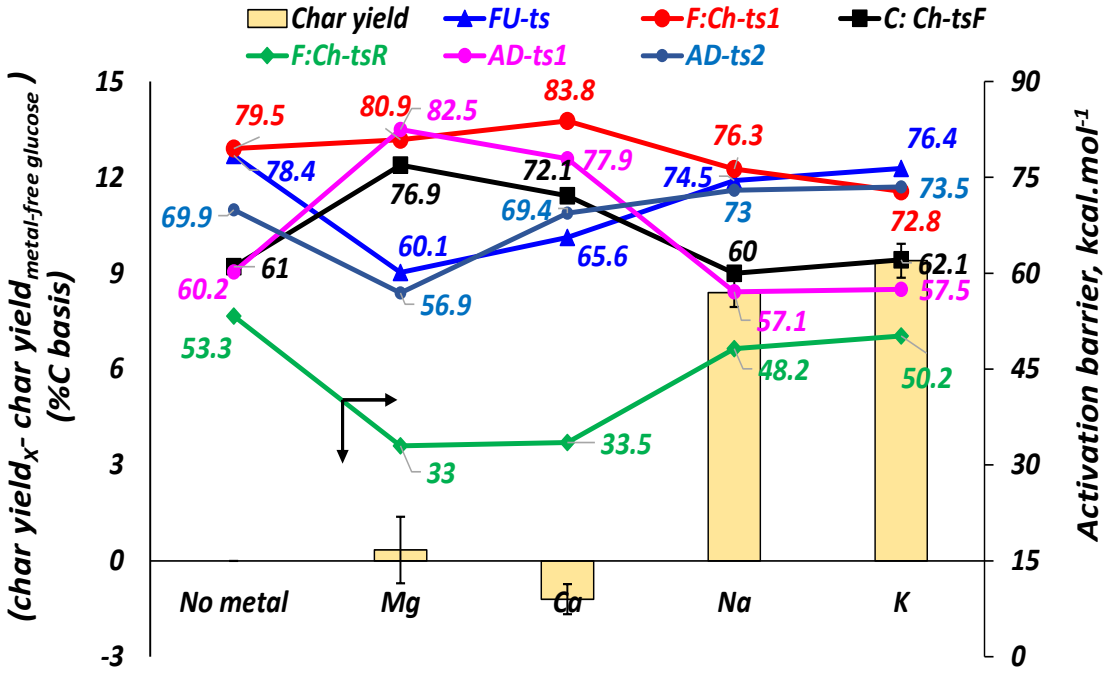

[B]

Figure 12: [**A**] Change in the yield of levoglucosan and C5 components with a corresponding variation in char yield in the presence and absence of alkali- and alkaline-earth metals [**B**] Correlation plot of the difference in char yield i.e., difference between the yields of char of metal-assisted (char yield$_x$) and metal-free conditions (char yield$_{\text{metal-free glucose}}$) with the activation enthalpies of ***a***) the reactions generating 1,2-anhydroglucopyranose (**5**) (AD-ts1 and Ch-tsR) and furfural (**19**) (FU-ts), ***b***) the rate-limiting step i.e., coupling reaction of 1,2-anhydroglucopyranose with nucleophile Ch-ts1 and ***c***) the competitive reactions of (**5**) having TSs Ch-tsF and AD-ts2, in the presence and absence of alkali- and alkaline-earth metal ions. Char yield in [**B**] is expressed as %C basis.

View Article Online
DOI: 10.1039/C9CY00005D

5. Conclusions

In this work, we used a combined approach of thin-film pyrolysis experiments and density functional theory (DFT) calculations to investigate the intrinsic reaction chemistry of glucose decomposition in the presence and absence of alkali- and alkaline-earth metal ions (AAEMs). The overall yields of bio-oil and char from thin-film pyrolysis of metal-free glucose were similar to that obtained from Mg(II)/glucose and Ca(II)/glucose. However, Na(I) and K(I) coordination decreased bio-oil yield by 2-6%, which, in turn, increased char yield by 9-10% compared to metal-free glucose. Further, looking at the individual bio-oil components from metal-free glucose pyrolysis, yield of 2,3-dihydro-3,5-dihydroxy-6-methyl-4H-Pyran-4-one (DHMDHP) was the highest followed by levoglucosan (LGA) and furfural. However, in the presence of metal cations, LGA yield was much higher than the yield of DHMDHP. For metal-assisted glucose pyrolysis, furfural yield was maximized in Mg(II)/glucose; levoglucoseneone (LGO) in Ca(II)/ glucose; 1,6-anhydroglucofuranose (AGF) in Na(I)/ glucose, while LGA in K(I)/ glucose. Hence, different metal ions have different effects on bio-oil composition.

The reactions leading to AGF, 1,5-anhydro-4-deoxy-D-glycero-hex-1-en-3-ulose (ADGH), LGA, LGO, 5-hydromethylfurfural, furfural, and char formation were investigated in the presence and absence of AAEMs. DFT calculations showed that AGF formation was catalyzed by the presence of Na(I) and K(I) ions, while Mg(II) and Ca(II) ions had an anti-catalytic effect. ADGH formation was favored in metal-free glucose, while all metal ions had an anti-catalytic effect. Further, the complexation of Mg(II) and Ca(II) ions had a catalytic effect on LGA formation, while decrease in the LGA yield was observed in the presence of Na(I) and K(I) ions. The decrease in LGA yield by Na(I) and K(I) ions were attributed to low activation enthalpies of LGA and furfural condensation reaction, favoring char formation, compared to metal-free system, while the presence of alkaline-earth metals promoted secondary reactions of LGA forming LGO. Thus, the fate of LGA was decided by the metal ion binding with LGA. Furthermore, Mg(II) and Ca(II) ions decatalyzed HMF formation, while Na(I) and K(I) ions had a neutral effect on the yield and activation barriers. Mg(II) and Ca(II) ions catalyzed furfural formation, while Na(I) and K(I) ions had an anti-catalytic effect.

Therefore, the difference in the catalytic effect of AAEMs on pyrolysis chemistry could be attributed to the difference in metal ion and donor atom(s) interaction within the transition state, which, in turn, altered the reaction kinetics. In summary, this work revealed that the yield and composition of bio-oil could possibly be tuned by using AAEMs.

Conflicts of interest

There are no conflicts to declare.

Supporting Information

Table S1 lists the complete product distribution of thin-film glucose pyrolysis at 200ºC in the presence and absence of alkali and alkaline-earth metal salts. Table S2 lists the activation enthalpy values as well as the free energies of activation of all the steps involved in formation of char and bio-oil components in the presence and absence of alkali and alkaline-earth metal ions. Tables S3-S10 list the electronic energy and free energy changes for LGA isomerisation, AGF formation, ADGH, LGA, LGO, 5-HMF, fufural and char formation. The values of electronic energy and free energy changes obtained in the present study are compared with the reactant (E and G = 0.0 kcal.mol^{-1}) and listed in Tables S3-S10 of the supporting information. The energies and atomic coordinates of all optimized reactants, intermediates and transition state structures of metal-free and metal-assisted glucose conversion reactions, are provided.

Acknowledgement

This research is supported by the Ministry of Education, Singapore, under the Academic Research Fund (AcRF) Tier-2 grant (Grant No. T2-1-082). Computational resources were provided by National Supercomputing Centre Singapore and Compute Canada.

References

1. X. Zhou, M. W. Nolte, H. B. Mayes, B. H. Shanks and L. J. Broadbelt, *Ind. Eng. Chem. Res.*, 2014, **53**, 13274-13289.
2. K. B. Ansari, J. S. Arora, J. W. Chew, P. J. Dauenhauer and S. H. Mushrif, *Energy Fuels*, 2018, DOI: 10.1021/acs.energyfuels.8b00852.
3. S. H. Mushrif, V. Vasudevan, C. B. Krishnamurthy and B. Venkatesh, *Chem. Eng. Sci.*, 2015, **121**, 217-235.
4. V. Agarwal, P. J. Dauenhauer, G. W. Huber and S. M. Auerbach, *J. Am. Chem. Soc.*, 2012, **134**, 14958-14972.
5. C. Zhu, C. Krumm, G. G. Facas, M. Neurock and P. J. Dauenhauer, *React. Chem. Eng.*, 2017, **2**, 201-214.
6. A. Banerjee and S. H. Mushrif, *ChemCatChem*, 2017, **9**, 2828-2838.
7. A. D. Paulsen, M. S. Mettler and P. J. Dauenhauer, *Energy Fuels*, 2013, **27**, 2126-2134.
8. M. S. Mettler, S. H. Mushrif, A. D. Paulsen, A. D. Javadekar, D. G. Vlachos and P. J. Dauenhauer, *Energy Environ. Sci.*, 2012, **5**, 5414-5424.
9. M. B. Pecha, J. I. Montoya, C. Ivory, F. Chejne and M. Garcia-Perez, *Ind. Eng. Chem. Res.*, 2017, **56**, 5185-5200.
10. Y. Xue, A. Kelkar and X. Bai, *Fuel*, 2016, **166**, 227-236.
11. M. S. Mettler, S. H. Mushrif, A. D. Paulsen, A. D. Javadekar, D. G. Vlachos and P. J. Dauenhauer, *Energy Environ. Sci.*, 2012, **5**, 5414-5424.

12. E. Hoekstra, W. P. M. Van Swaaij, S. R. A. Kersten and K. J. A. Hogendoorn, *Chem. Eng. J.*, 2012, **187**, 172-184.
13. C. Krumm, J. Pfaendtner and P. J. Dauenhauer, *Chem. Mater.*, 2016, **28**, 3108-3114.
14. C. Zhu, C. Krumm, G. G. Facas, M. Neurock and P. J. Dauenhauer, *React. Chem. Eng.*, 2017, **2**, 201-214.
15. S. Maduskar, G. G. Facas, C. Papageorgiou, C. L. Williams and P. J. Dauenhauer, *ACS Sustain. Chem. Eng.*, 2018, **6**, 1387-1399.
16. C. Krumm, J. Pfaendtner and P. J. Dauenhauer, *Chem. Mater.*, 2016, **28**, 3108-3114.
17. E. Leng, M. Costa, Y. Peng, Y. Zhang, X. Gong, A. Zheng, Y. Huang and M. Xu, *Fuel*, 2018, **234**, 738-745.
18. J. B. Paine, Y. B. Pithawalla and J. D. Naworal, *J. Anal. Appl. Pyrolysis*, 2008, **82**, 42-69.
19. J. C. Degenstein, P. Murria, M. Easton, H. Sheng, M. Hurt, A. R. Dow, J. Gao, J. J. Nash, R. Agrawal, W. N. Delgass, F. H. Ribeiro and H. I. Kenttamaa, *J. Org. Chem.*, 2015, **80**, 1909-1914.
20. B. Hu, Q. Lu, X.-y. Jiang, X.-c. Dong, M.-s. Cui, C.-q. Dong and Y.-p. Yang, *Energy Fuels*, 2017, **31**, 8291-8299.
21. X. Zhou, M. W. Nolte, H. B. Mayes, B. H. Shanks and L. J. Broadbelt, *Ind. Eng. Chem. Res.*, 2014, **53**, 13274-13289.
22. R. Vinu and L. J. Broadbelt, *Energy Environ. Sci.*, 2012, **5**.
23. V. Seshadri and P. R. Westmoreland, *J. Phys. Chem. A*, 2012, **116**, 11997-12013.
24. H. B. Mayes, M. W. Nolte, G. T. Beckham, B. H. Shanks and L. J. Broadbelt, *ACS Sustain. Chem. Eng.*, 2014, **2**, 1461-1473.
25. H. B. Mayes, M. W. Nolte, G. T. Beckham, B. H. Shanks and L. J. Broadbelt, *ACS Catal.*, 2014, **5**, 192-202.
26. C. Zhu, S. Maduskar, A. D. Paulsen and P. J. Dauenhauer, *ChemCatChem*, 2016, **8**, 818-829.
27. P. R. Patwardhan, J. A. Satrio, R. C. Brown and B. H. Shanks, *Bioresource Technol.*, 2010, **101**, 4646-4655.
28. N. Shimada, H. Kawamoto and S. Saka, *J. Anal. Appl. Pyrolysis*, 2008, **81**, 80-87.
29. Y. Yu, D. Liu and H. Wu, *Energy Fuels*, 2013, **28**, 245-253.
30. P. R. Patwardhan, J. A. Satrio, R. C. Brown and B. H. Shanks, *J. Analy. Appl. Pyrolysis*, 2009, **86**, 323-330.
31. P. R. Patwardhan, D. L. Dalluge, B. H. Shanks and R. C. Brown, *Bioresour. Technol.*, 2011, **102**, 5265-5269.
32. J. S. Arora, J. W. Chew and S. H. Mushrif, *J. Phys. Chem. A*, 2018, **122**, 7646-7658.
33. S. Maduskar, V. Maliekkal, M. Neurock and P. J. Dauenhauer, *ACS Sustain. Chem. Eng.*, 2018, **6**, 7017-7025.

34. M. J. Frisch, G. W. Trucks, H. B. Schlegel, G. E. Scuseria, M. A. Robb, J. R. Cheeseman, G. Scalmani, V. Barone, B. Mennucci and G. A. Petersson, et al., *Journal*, 2009, DOI: citeulike-article-id:9096580.
35. M. S. Mettler, A. D. Paulsen, D. G. Vlachos and P. J. Dauenhauer, *Energy Environ. Sci.*, 2012, **5**.
36. H. B. Mayes and L. J. Broadbelt, *J. Phys. Chem. A*, 2012, **116**, 7098-7106.
37. A. Saddawi, J. M. Jones and A. Williams, *Fuel Process. Technol.*, 2012, **104**, 189-197.
38. S. H. Mushrif, J. J. Varghese and D. G. Vlachos, *Phys. Chem. Chem. Phys.*, 2014, **16**, 19564-19572.
39. A. Trendewicz, R. Evans, A. Dutta, R. Sykes, D. Carpenter and R. Braun, *Biomass Bioenergy*, 2015, **74**, 15-25.
40. B. Hu, Q. Lu, X.-y. Jiang, X.-c. Dong, M.-s. Cui, C.-q. Dong and Y.-p. Yang, *Energy Fuels*, 2017, **31**, 8291-8299.
41. R. S. Assary and L. A. Curtiss, *ChemCatChem*, 2012, **4**, 200-205.

Graphical Abstract

View Article Online
DOI: 10.1039/C9CY00005D

Alkali and alkaline-earth metal loaded biomass pyrolysis highlights that different metal ions have different effects on bio-oil composition.